Exploring a Finite Wind Farm for Partial Repowering by Vertical Staggering of Low Performing Horizontal Axis Wind Turbines

By

Mehtab Ahmad Khan

Reg # 00000273378

Session 2018-2020

Supervised by

Dr. Sehar Shakir

A Thesis Submitted to the US Pakistan Centre for Advanced Studies in Energy in partial fulfillment of the requirements of the degree of

MASTERS of SCIENCE in

ENERGY SYSTEMS ENGINEERING

US-Pakistan Centre for Advanced Studies in Energy (USPCAS-E)

National University of Sciences and Technology (NUST)

H-12, Islamabad 44000, Pakistan

March 2021

THESIS ACCEPTANCE CERTIFICATE

Certified that final copy of MS/MPhil thesis written by **Mr. Mehtab Ahmad Khan** (Registration No. 00000273378), of USPCAS-E has been vetted by undersigned, found complete in all respects as per NUST Statues/Regulations, is within the similarity indices limit, and is accepted as partial fulfillment for the award of MS/MPhil degree. It is further certified that necessary amendments as pointed out by GEC members of the scholar have also been incorporated in the said thesis.

Signature: _____

Name of Supervisor Dr. Sehar Shakir

Date: _____

Signature: _____

Name of Co-Supervisor Dr. Adeel Javed

Date: _____

Signature (HoD ESE): _____

Date: _____

Signature (Dean/Principal): _____

Date: _____

Certificate

This is to certify that work in this thesis has been carried out by **Mr. Mehtab Ahmad Khan** and completed under my supervision in US-Pakistan Center for Advanced Studies in Energy (USPCAS-E), National University of Sciences and Technology, H-12, Islamabad, Pakistan.

Supervisor: _____

Dr. Sehar Shakir
USPCAS-E
NUST, Islamabad

Co-Supervisor: _____

Dr. Adeel Javed
USPCAS-E
NUST, Islamabad

GEC member 1: _____

Dr. Majid Ali
USPCAS-E
NUST, Islamabad

GEC member 3: _____

Dr. Warda Ajaz
USPCASE
NUST, Islamabad

HOD-ESE: _____

Dr. Naseem
USPCAS-E
NUST, Islamabad

Principal: _____

Dr. Adeel Waqas
USPCAS-E
NUST, Islamabad

Dedication

I dedicate my thesis to my mother only for always believing in me, praying for me, and giving me courage.

Abstract

Vertical staggering (VS) of horizontal axis wind turbines is explored to eliminate the effects of inter-farm wakes and partially repower the existing arrays for enhanced power production. Nine turbines of the FFCEL wind farm of Jhimpir, Pakistan were considered for a micro-scale numerical study; these turbines were identified as the most affected ones by a mesoscale numerical simulation for the same site. A RANs model was employed to simulate the flow through a domain that acquired boundary condition data from the results of the WRF study for the wind farm under consideration. Furthermore, the convective atmospheric boundary layer was also considered for the investigation. The hub heights were changed from 80 m to both 60 m and 100 m in separate cases. By elevating the turbines to 100 m the cumulative power extraction of the 9 turbines increased by 13.5 % and reducing the hub height to 60 m decreased the power output by 11.5 % of that of the current configuration. The effect of the compound wakes appeared mild at 100 m, modest at 80 m, and high at 60 m; as the maximum velocity deficit observed under the influence of compound wakes is 13.26 %, 14.06 %, and 15.17 %, respectively. The comparison of wake recovery for neutral atmospheric boundary conditions with that of the convective atmospheric boundary layer revealed the latter to speed up the wake recovery. The lateral repositioning of some of these turbines was also performed for the 100 m case. The power generation of the laterally optimized layout at 100 m hub height was 23 % more than that of the existing layout. Therefore, the increase of the hub heights of onshore horizontal axis wind turbines proves to be an affordable strategy to partially repower finite wind farms affected by compound wakes.

Keywords: Wind farm; repowering; mesoscale simulation; wake interference; hub height variation; model validation

Table of Contents

List of figures

List of Tables

List of journal papers/conference papers

1. **Partial Repowering Analysis of a Wind Farm by Coupled Actuator Disk and Mesoscale Models to Mitigate Neighboring Wind Farm Wake Interference**
   Mehtab Ahmad Khan[a], Adeel Javed[a,1], Sehar Shakir[a], Abdul Haseeb Syed[b]
   [a]U.S.-Pakistan Centre for Advanced Studies in Energy (USPCAS-E), National University of Sciences and Technology (NUST), H-12 Islamabad, Pakistan
   [b]Department of Wind Energy, Technical University of Denmark (DTU), Roskilde, Denmark. First revisions invited by Applied Energy.

List of Nomenclature

A	Rotor Area [m^2]
a	Axial induction factor
C_P	Power Coefficient [-]
D	Rotor Diameter [m]
F_A	Force exerted by the rotor on wind [N]
g	Gravitational acceleration [ms^{-2}]
H	Height [m]
H_{hub}	Hub Height [m]
P_{rated}	Rated Power [W]
$P_{2.b}$	Pressure just aft of the actuator disk [Pa]
$P_{2.f}$	Pressure just in front of the actuator disk [Pa]
P	Pressure [Pa]
Q_{net}	Total heat exchange across the control surface [J]
t	Time [s]
V	Horizontal wind speed [ms^{-1}]
ABL	Atmospheric Boundary Layer
ADM	Actuator Disk Modeling
ALM	Actuator Line Modeling
ASM	Actuator Surface Modeling
AEP	Annual Energy Production
C-ABL	Convective Atmospheric Boundary Layer
CFD	Computational Fluid Dynamics
HAWT	Horizontal Axis Wind Turbine
LES	Large Eddy Simulation
N-ABL	Neutral Atmospheric Boundary Layer
NWP	Numerical Weather Prediction
RANS	Reynolds Average Navier-strokes
TKE	Turbulent Kinetic Energy
VAWT	Vertical Axis Wind Turbine
WRF	Weather Research and Forecasting
WTG	Wind Turbine Generator

Chapter 1
Introduction

1.1 Background

The quest of many countries to harness energy from renewable resources like the wind is booming rapidly than ever before. By 2020 wind energy contributed 650.8 GW to the energy mix of the globe [1]. Much of this wind energy share comes from developed countries and the developing countries add lesser. However, the rapid growth of the wind sector across the globe is constraint by a span of challenges, which include expensive technology, distributed nature of wind resources, limited sites with sufficient wind speed, and relatively low power density of wind farms.

Pakistan has also shown sheer commitment to harness the acute wind resources it has got in Sindh and along some of its coastal lines [2]. The limited onshore wind sites are one of the major constraints of the overall wind capacity of the country. This is because the horizontal axis wind turbines (HAWTs) deployed in arrays require significant gaps between the rows of turbines [3] and thus much of the site is left empty. Although, careful positioning of the individual turbines in the wind farm maximizes the energy output still much of the wind, especially below the lower tip of the HAWT is not utilized [4].

The concept of vertical staggering (VS) seems a viable solution to extract most of the wind energy from a farm. As shown in figure 1, a vertically staggered configuration of wind turbines could be a combination of any two or more of the wind generators in the figure. The turbines placed at different heights capture much of the site area to confront a smoother wind field than that of a conventional wind farm. A relatively emerging idea like VS of HAWTs is to utilize both HAWTs and Vertical Axis Wind Turbines (VAWTs). The smaller and shorter VAWTs can operate below the rotors of the HAWT and can be scattered among the gaps of the HAWT. This is deemed to increase the power density and recover the velocity in the wake of the HAWTs quickly [4].

The wind is a distributed form of renewable energy resource available in sufficient magnitude for harvest only in specific regions like coastal lines and corridors. The use of

wind turbines in arrays instead of individual machines has been more trending across the globe in the last few decades. However, the configuration of the wind turbines in wind farms is constraint by cost, land, wind resource, and most importantly the wakes produced by the upstream turbines behind them. Generally, the velocity deficit and turbulence caused by the upfront turbines cause reduced power output and increased structural loads on the downstream turbines.

It is common in the wind industry to conduct experimental measurements of wind speed and directions on a site before setting up a wind farm. However, the wakes produced by individual turbines and their interaction with other rotors can be predicted either by analytical or numerical models. Together the above two major assessments lead to an optimized layout of a wind farm to be installed. Unfortunately, the latter part is underestimated in developing countries like Pakistan, and therefore there exist wind farms that are not optimized and hence operate with low efficiencies.

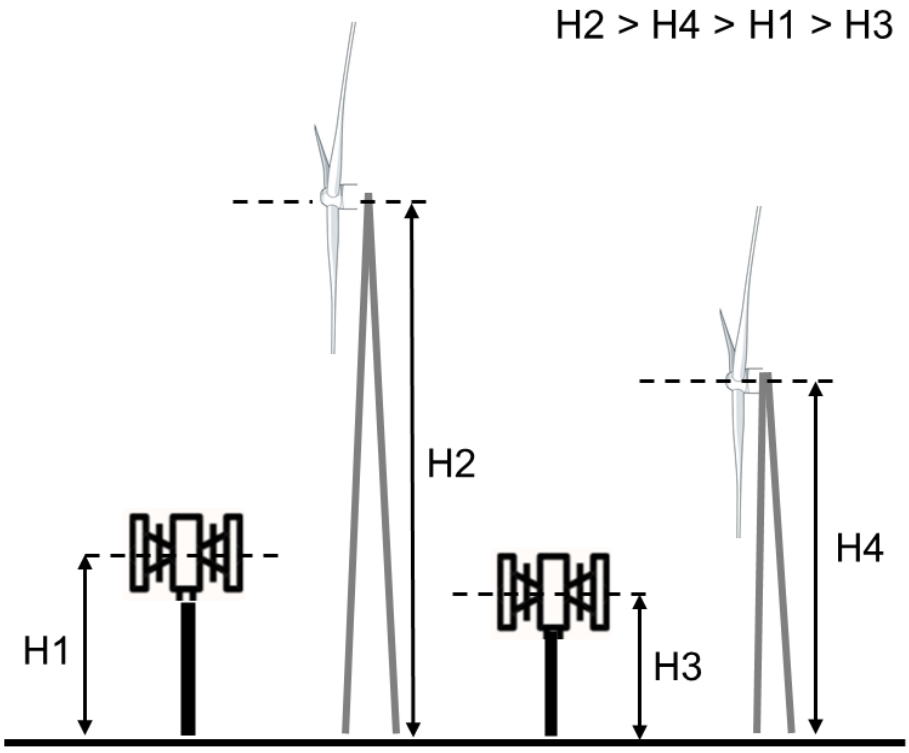

Figure 1.1: A schematic representation of vertical staggering.

1.2 Research gap

As shown in figure 1.2, the FFCEL wind farm operated behind TGF and ZORLU. The distances among these wind farms are small, which indicates the compound wakes of the upstream wind farms falling onto the FFCEL wind farm. Further, within the FFCEL some turbines are aligned in the direction of the dominant winds. Together these two situations result in the low performance of the wind farm.

As these wind farms approach the end of their life, the chances of repowering are evident. Full repowering schemes might not be affordable and convenient, which invites the opportunity to explore partial repowering strategies to both enhance the power output and extend the life of the wind farm. Among some of the recently introduced partial repowering schemes, the mesoscale numerical models are notable for their ability to include the effects of wind turbines on flow through wind farms. It is also thought to be effective to depict the variations of flow in the atmospheric boundary layer. However, the spatial resolution of the mesoscale models is low and that becomes a constraint when it comes to simulating flow to assess the effects of wakes of individual turbines on the flow and downstream turbines. Microscale numerical modeling is most suitable to study the flow interactions with high resolution, but it comes with a high computational cost. Thus, the numerical modeling of wind farms requires actuator models to reduce the computational cost. This is a trade-off between the accuracy and affordability of microscale numerical simulations. Atmospheric boundary conditions are equally important to incorporate in a numerical study but that is a complicated procedure that requires specific attention.

In the given scenario a hybrid method is proposed in this thesis, which manually couples the WRF model with a CFD model. The incorporation of an actuator disk model for creating effects like a wind turbine is proposed to keep the method simple. Further, convective atmospheric conditions are also implemented to ensure realistic flow conditions [5].

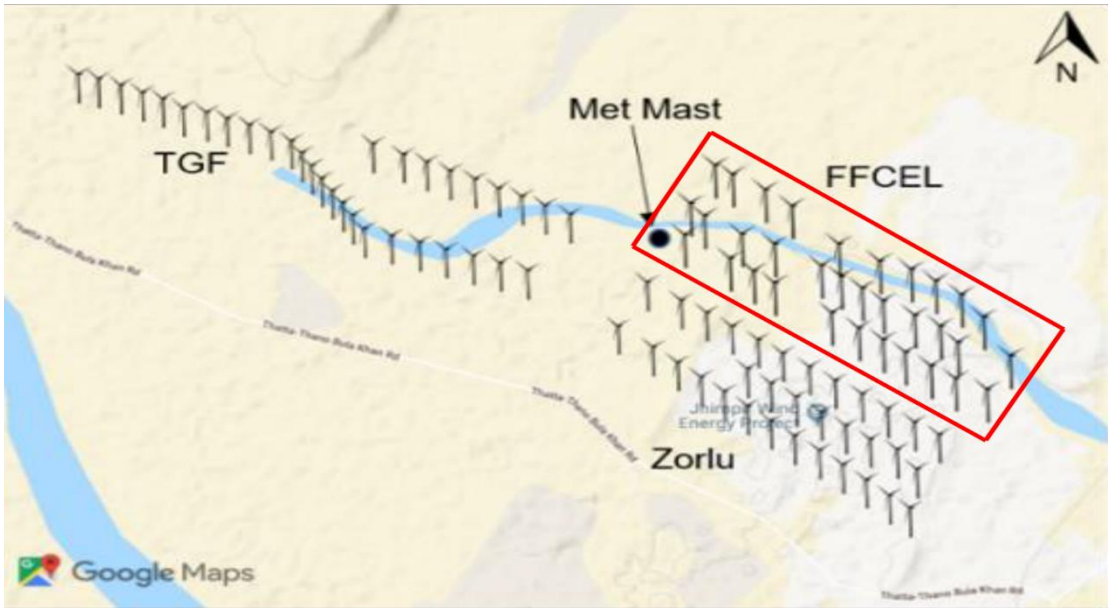

Figure 1.2: Representation of FFCEL, TGF and ZOURLU wind farms in Jhimpir, Sindh.

1.3 Aims and objectives.

Mainly, this thesis aims to evaluate the current layout of the FFCEL wind farm for the effects of wakes coming from the upstream wind farms on it. Since any newly proposed layout would be restricted by available land and density of wind turbines, thus the major objective would be to propose a vertically staggered layout for the expected mid-life repowering of the wind farm. ANSYS FLUENT would be the major tool to conduct the simulations on the models developed to achieve the above-mentioned objectives.

Since the numerical simulation of complete wind farms is computationally expensive and time-consuming, it is important to split the task in hand into various separate steps as enlisted below:

- Develop a model to acquire the flow properties as inputs for the FFCEL wind farm from the upstream wind farms.
- Devise an actuator disk model for the CFD of some of the most affected wind turbines from the FFCEL wind farm.
- Establish vertically staggered layouts of the previously studied wind turbines to improve the power production of those turbines.
- Validate the results from previous steps with experimental results from the existing configuration.

1.4 Present work

The chapters to follow are briefly described below:

Chapter 2 would cover the literature review of the most relevant research on wind farm wakes and their effects. The review would look up various modeling techniques for wake development and interactions, power loss due to velocity deficit in the wake, and optimization of wind farms by the vertical staggering of the turbines.

In Chapter 3, the numerical models for wind farm modeling would be overviewed to opt for the suitable models to evaluate and simulate the FFCEL wind farm wakes. The Actuator disk modeling of the wind turbines will be addressed comprehensively since it would be central to the numerical simulation of the wind farm. A brief mention of the atmospheric boundary layer and the wind flow over various terrains would also be part of this section of the thesis.

Chapter 4 would be dedicated to the detailed CFD methodology of the model. The implementation of Actuator disk modeling by porous-media boundary conditions in Fluent would be described. Further, the creation of the domain, the choice of turbulent model, setting up appropriate boundary conditions, the numerical discretization schemes, and other solver setups would be explained. The validation and verification of the numerical setup and the solution would be presented towards the end of this chapter.

Chapter 5 would present the results from the numerical simulations of both the present layout and the proposed configuration of the wind turbines in the FFCEL wind farm. The results would be compared with those from the analytical modeling of the wind farm cases and the experimental data from the present wind farm. This would bring us to the conclusion of this research and hence a summary of major findings and further possibilities of research will be discussed.

Appendix A provides the boundary condition profiles developed to interpolate the flow data of WRF simulations for FFCEL wind farms to the domain of CFD analysis.

Summary

This chapter describes the background of this thesis work. The share of wind energy in the energy mix of the planet is highlighted to assert its potential to grow in near future. Some of the common technologies used in the wind industry are HAWTs and VAWTs. The arrays of HAWTs are more trending across the globe and the constraints on gaps between rows of turbines is a critical challenge to address. The distributed nature of wind resources demands the efficient utility of wind corridors. Hence, concepts like vertical staggering can prove handy to enhance the power densities of wind farms. A vertically staggered wind farm has rotors placed are variable hub heights and therefore can prove significant in repowering under-performing wind farms. The turbulence caused by upstream wind turbines can be avoided by placing downstream turbines at different heights than the upfront ones. Thus, this chapter sets the goals and objectives of the research to investigate the vertically staggered wind farms for enhanced power production and reduced effects of the compound wakes. The layout of research activities to be reported is briefly described in the last section of this chapter.

References

[1] "Global Wind Power Statistics – Wind Energy International Platform." https://library.wwindea.org/global-statistics/ (accessed Nov. 20, 2020).

[2] D. Elliott, "SOUTH ASIA REGIONAL INITIATIVE FOR ENERGY COOPERATION AND DEVELOPMENT (SARI-Energy) Wind Resource Assessment and Mapping for Afghanistan and Pakistan."

[3] J. O. Dabiri, "Potential order-of-magnitude enhancement of wind farm power density via counter-rotating vertical-axis wind turbine arrays," *J. Renew. Sustain. Energy*, vol. 3, no. 4, 2011, DOI: 10.1063/1.3608170.

[4] S. Xie, C. L. Archer, N. Ghaisas, and C. Meneveau, "Benefits of collocating vertical-axis and horizontal-axis wind turbines in large wind farms," *Wind Energy*, vol. 20, no. 1, pp. 45–62, Jan. 2017, DOI: 10.1002/we.1990.

[5] A. H. Syed, A. Javed, R. M. Asim Feroz, and R. Calhoun, "Partial repowering analysis of a wind farm by turbine hub height variation to mitigate neighboring wind farm wake interference using mesoscale simulations," *Appl. Energy*, vol. 268, p. 115050, Jun. 2020, DOI: 10.1016/j.apenergy.2020.115050.

Chapter 2

Literature Review

2.1 Development of wind turbines and wind farms

Wind turbines are engineering marvels that make use of theories of aerodynamics, mechanics, and electromagnetism to harvest and convert the kinetic energy of wind into electrical energy. The use of Windmills; for grinding grain, pumping water, and more recently to produce electricity, is known to humans for a few centuries now. Wind turbines can be classified based on the force that drives their rotors and the Axis of rotation of the rotor. Generally, we regard the classification of wind turbines based on their axis of rotation. Horizontal Axis Wind Turbine (HAWT) has its rotation axis parallel to the ground and the other type has its rotation axis perpendicular to ground and hence termed as Vertical Axis wind turbine (VAWT). HAWTs are generally lift-driven, whereas VAWTs can be both lift-driven and drag-driven but generally smaller and less efficient than HAWTs. The schematic diagrams of horizontal axis wind turbines and various types of vertical axis wind turbines are given in figure 2.1 and figure 2.2.

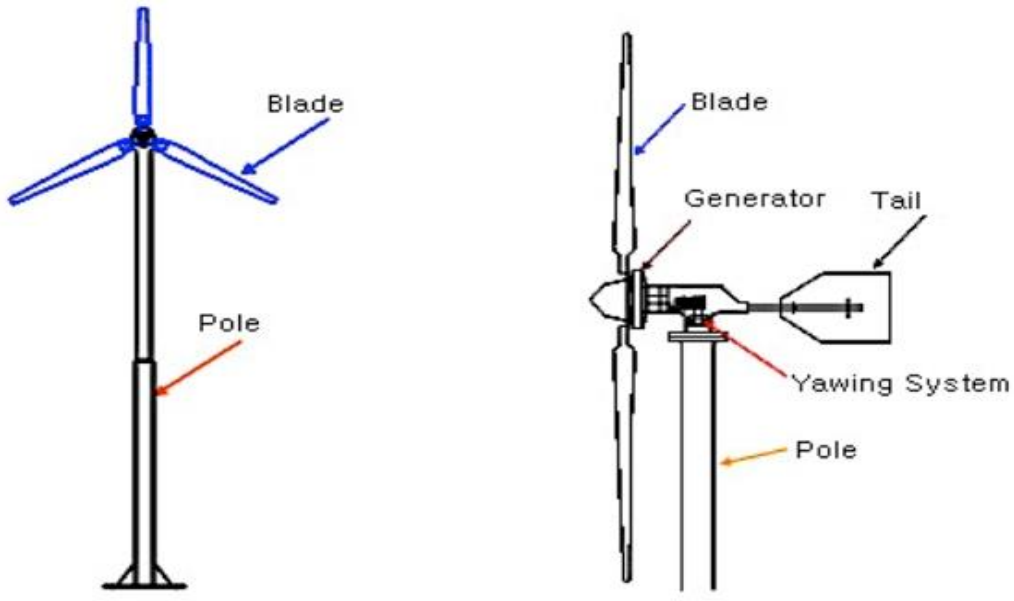

Figure 2.1: Schematic of a horizontal axis wind turbine (HAWT) [1].

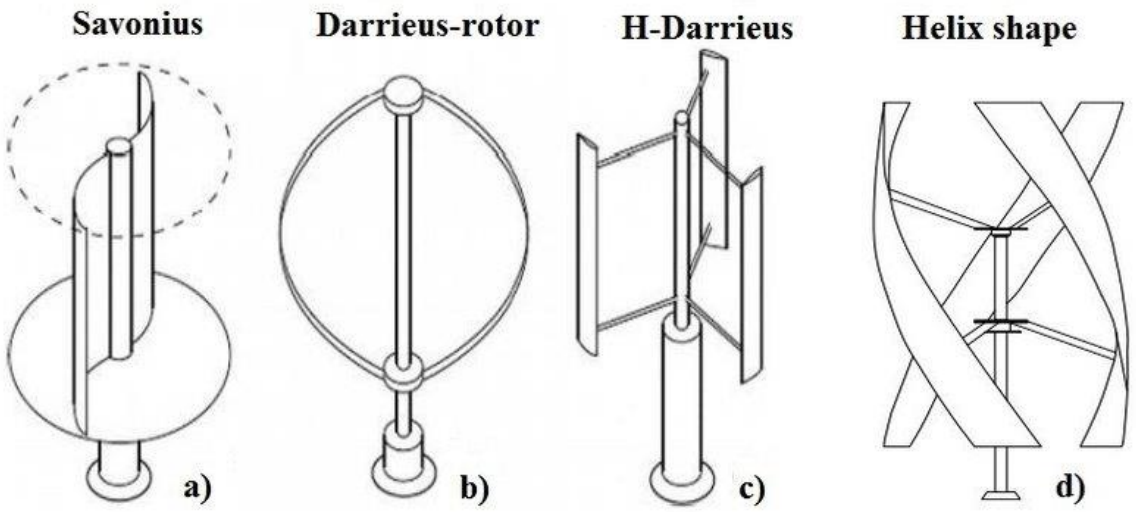

Figure 2.2: Schematic diagrams of major types of vertical axis wind turbines [2].

Wind turbines have evolved rapidly, and the associated technologies have matured now. It was Pou La Cour who invented the first electricity-producing wind turbine in 1891 and ever since these machines have kept advancing in both size and efficiency. The largest wind turbine in the world by 2020 is installed by General Electric on an offshore site in Rotterdam that has a rated power of 12 MW, a hub height of 107 m, and a rotor diameter of 220 m. The installed capacity of wind energy across the globe had exceeded 486 GW by 2016 and most of it is harvested by HAWTs that are deployed in wind farms. Over the last few decades, wind arrays have been established on offshore sites. However, there are various onshore sites across the globe with huge wind resources and hence onshore wind farms do have a significant share in the overall wind energy production.

Wind turbines are designed and optimized to achieve higher efficiencies but the best efficiency that any wind turbine can ever achieve is 16/27; known as the Betz's Limit determined by Albert Betz in 1919 [3]. The blades of a wind turbine are the most important parts with regards to its efficiency. Airfoil is a cross-section of a blade, which determines the shape and more significantly the aerodynamics of the blade. Airfoils of helicopters were the first choice of wind turbine developers, but more recently special airfoils are designed to meet the structural and aerodynamic needs of the wind turbines. For the larger HAWTs, it is a common practice to use at least two airfoils on a blade. To ensure resilience against the high bending moments at the hub of a turbine, thicker airfoils are used.

Whereas the airfoils towards the tips are thinner to reduce the overall weight of the blade. Similarly, the blades are also tapered towards the tips to ensure uniformity of the lift force over the blade span. Since the sections of the blade closer to the hub have lower tangential velocities and produce lower lift than that of the sections towards the tips. To improve the hub section's lift, they are twisted to provide a higher angle of attack.

The wind speed and direction keep changing even at a given site. This requires further arrangements on a HAWT to ensure optimal performance of the machine throughout its operational life. Thus, it is common among the HAWTs to have a pitch controller that changes the angle of incidence of the wind to acquire suitable aerodynamic forces on the blades. Likewise, the yaw motor sits on top of the pole to align the rotor into the inflow of the wind all the time. The turbine nacelle of a HAWT also sits atop the pole that contains the electric generator and various other mechanical and electronic equipment. The pole hosts the nacelle and the rotor high up in the air stream that is smoother and faster than that closer to the ground.

Installing individual HAWTs has always been overlooked to opt for their arrangement in arrays. A wind turbine operating individually at a site might be more efficient than the same one operating in a wind farm. Since wind is available on specific sites, the concept of deploying groups of closely placed wind turbines can provide higher power than that of placing individuals. Thus, the concept of wind farms of HAWT has been booming over the last century. Wind farms were first introduced in the early 19^{th} century and since then the concept has evolved to great extent. Currently, there are hundreds of wind farms, both onshore and offshore, across the globe. The largest one is in Gansu, China that has a target of achieving 20,000 MW power output by 2020.

More recently researchers have attempted to use VAWTs in arrays. For their low efficiencies compared with HAWTs, VAWTs have been ignored. It was until 2010 when VAWTs were tested for their performance in the grouped form and incredibly their power outputs were reported to exceed that of isolated cases. Another research found groups of counter-rotating turbines to produce higher power than those rotating in the same direction. Mostly, the VAWTs are smaller than HAWTs and therefore they require lesser land to install. Thus, the power density of VAWT is much higher than that of HAWT.

Unlike HAWTs, they perform better in turbulent winds and do not require any provisions to align with the direction of the wind. It is common to install VAWTs in urban conditions, on rooftops, and in buildings. The latest concept is to use VAWTs behind HAWTs in the existing wind farms. This has been reported to increase the power density of the wind farm and improve the wake recovery of the HAWTs.

2.2 Wind turbine wakes

As the wind turbines consume some of the kinetic energy of the wind, it is expected for the flow downstream to have a lower velocity. Likewise, the blockage of the flow by the blades and the induction of velocity components due to their rotation has a significant impact on the downstream flow. All these effects in the flow stream to the rear of a wind turbine are termed as the wake. Therefore, a wake is simply the region behind the turbine that is both deficient in velocity and increase turbulence.

Wakes have adverse effects on the turbines of a wind farm that operate downstream of the upfront rotors. Lower power outputs from the turbines operating in wakes are a major flaw caused by the deficiency of kinetic energy. The power loss of wind farms depends on the layouts and the range of energy loss is 5 % to 15 % [4]. The higher intensity of turbulence in awake would increase structural loads, leading to increased maintenance costs and reduce lifetimes.

Generally, the turbine wake is split into two regions: the near and far wake. The region adjacent to the turbine is the near wake, which is directly influenced by the geometry of the rotor. The pressure drop across the rotor is the major source of the velocity deficit and hence the near wake. Most of the literature reports the near wake to extend up to 4D downstream [5], [6], [7]. Some other research finds the length of the near wake to reach lengths of just 1D [8]. The far wake on the other hand might recover after 10D to 15D downstream. Unlike near wake, far wake depends on the topography of the site, turbulence dissipation, and wind shear in the atmospheric boundary layer.

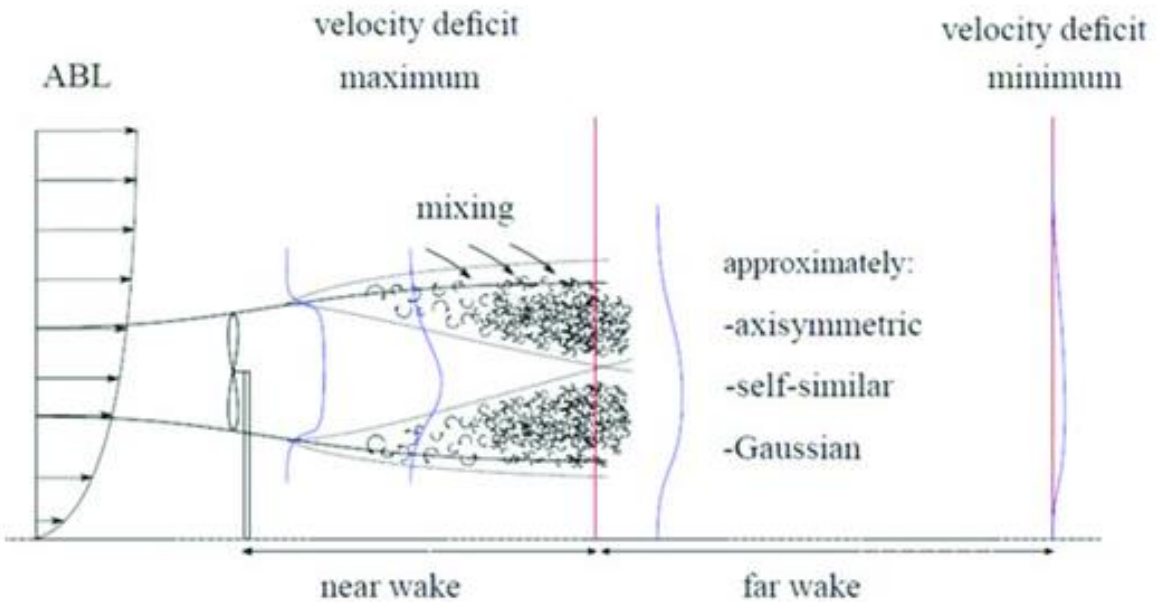

Figure 2.3: The behavior of wake behind a HAWT in ABL [9].

2.2.1 Near wake

A close inspection of the near wake reveals a huge plunge in pressure right across the blades and a good fraction of velocity is extracted to cause a low-velocity zone. As the flow progresses downstream, the pressure would rise to catch up with the ambient pressure. This at the same time causes to further decrease in the velocity and the lowest speeds are therefore reported in near wake at downstream distances of 1D to 2D [6]. Outside the rotor flow stream, the velocity is still higher and thus a high-velocity gradient establishes between the near wake and the faster outer flow. The zone of this high-velocity slope develops into a sheared layer of large turbulent eddies. The turbine wake always interacts with the atmospheric boundary layer, which has an asymmetric profile in the vertical plane due to the ground effect. Hence the sheared layer above the hub height has higher turbulent intensity compared with that of the shear layer formed below the hub height. Although these shear layers cause turbulence they are critical to the recovery of the velocity deficit. The large eddies in the shear layers allow the outer fast traveling flow to mix with the slower flow inside the wake. This transfer of kinetic energy eventually overcomes the adverse velocity drop in the near wake. The outer flow gradually expands and more prominently towards the axis of the rotor. The inwards expanding shear layer would assume a different behavior upon reaching the rotor axis and hence the near wake ends at this location.

The geometry of the turbine and especially the blade contribute to the turbulence of the near wake and it is termed mechanical turbulence. The flow is both blocked and reoriented in various directions by various parts (tower, nacelle, and blades) of the turbine, which creates a chaotic flow in the near wake. The blades, just like any aerodynamic object shed vortices from their trailing edges and much stronger helical vortices from the tips. These vortices develop into a turbulent rotating sheet as they progress downstream and the ambient turbulence in the wind itself helps deplete the vortices. The ambient turbulence or the turbulence carried by the wind itself also adds a small share to both the near and far wakes.

2.2.2 Far wake

The far wake differs from the near wake in many ways. The near wake is more significant regarding the performance of the turbine. However, the far wake is more relevant for wind farm studies. The flow recovery depends more on the ambient turbulence, which allows the mixing of the slower flow in the wake with faster flow outside of it. Although, the parabolic profile of wind in the atmospheric boundary layer (ABL) is critical to the recovery of the flow. Excluding the effect of ABL, the far wake appears symmetric in a cross-section parallel to the rotor plane. The far wake does expand as it progresses downstream, but it becomes weaker. It is unrealistic to ignore the topographic effects on the ABL and hence in the far wake the velocity recovery is slower below the rotor hub heights and above it, the velocity deficit dies down quicker due to higher turbulence intensity. It has also been observed that the wake develops wider in the upward direction than the downward direction. Turbulence in the far wake is helpful in the recovery of velocity but it is undesirable for the turbines operating in the downstream direction. A major concern related to turbulence is the increased loading on the turbines. Another research also confirms that the velocity deficit recovers faster than the turbulence in the wakes [10].

2.3 Wake modeling of wind turbines

The above section made it obvious that wake behind a wind turbine assumes various behaviors as the flow sweeps downstream and therefore it can have different impacts on the performance of any other wind turbine in the wake, depending on its downstream

distance. Further, it was also established that far wake studies are more important for wind farm layout optimization. Therefore, this section of the present chapter would focus on major make modeling techniques used till the time to assess the far wakes of HAWTs.

Generally, a wake model would be a set of mathematical relationships that are developed based on the physics of fluid flow over a stationary but rotating body. These expressions would be functions of flow properties, like velocity, density, viscosity, and pressure, etc. Although, the rotors of wind turbines are carefully designed aerodynamic components still they will have an impact on the flow striking and/or sweeping past them. Therefore, some mathematical expressions would link these impacts of turbine geometry on the flow. Similarly, some relationships would take care of the terrain on the atmospheric boundary layer and further the interaction of ABL with the wakes. Altogether, these sets of equations would intend to provide the velocity profile and turbulence intensity in the wake of the turbine; a set of such relationships is termed as a wake model.

Some researchers initially developed analytical models but later as the computers grew powerful, different solvers were developed to solve the complete flow equations for the flow over a body. Thus, the computational models, which are usually not specific to a particular fluid problem and include various turbulence models, have now emerged as more accurate tools to study the wakes of turbines. Therefore, the models to analyze the wakes of wind turbines can either be analytically or numerically [11]. Analytical models are developed on the concept of energy content in the flow field and do not include the detailed behavior of the flow [12], [13]. These models predict the velocity deficit in the wake of the turbines and exclude the turbulence unless a separate turbulence model is included when necessary. On the other hand, the computational models solve the complete Navier-Stokes equations for the considered flow field domain. Numerical models are robust and provide a deeper insight into the velocity deficit and turbulence intensity in the wake. However, the resolution and accuracy of the solution provided are directly dependent on the computational power and time.

2.3.1 Kinematic models

The focus of this thesis is to study the far wakes. The most used far wake models are grouped into two major types: the kinematic models [14], field and wake eddy turbulence

model models [15], [16], [17]. Whether solved analytically or numerically through some software the Kinematic models cater for the conservation of momentum only. This infers that the velocity deficit in the wake is the main output of these models and the variations in turbulence are not included unless a separate turbulence model is solved for the given flow field [18]. In concept, kinematic models are based on self-similar velocity variations in co-flowing jets of fluid. Some of the major models that fall under kinematic models are Jensen's wake model, Larsen wake model, and Frandsen wake model. A brief overview of these models is given in the following section.

The park model or Jensen's wake model is the head starter of wake studies of wind turbines. It was developed by N.O. Jensen [16] and improved by Katic [13]. This model is further classified into a single wake model and a multiple wake model. The model is built on the principle of conservation of momentum downstream of the turbine and thus it evaluates the velocity profile as a function of only the distance in the wake of the turbine. It also considers the expansion of the wake by assuming it linear but neglects the vortices shedding from the tips and trailing edges of the turbine blades. This last feature makes it suitable for the far wake studies only. Interestingly, this model also considers the terrain of the wind farm by assigning some coefficients that depict the impacts of the roughness of the ground on the wake. By incorporating the coefficient of the thrust of the upwind turbines, this model somehow entertains the energy extraction effects of the turbine on to flow behind it.

For a single wake model, the velocity profile is relatively simple, and it appears 'hat-shaped'. On the other hand, the multi wake model is much more complicated as it must depict the interaction of various wakes from many turbines on a farm. Since the interaction of wakes can have various patterns and therefore the velocity at any point in the interacting wake is dependent on the shadowing. The multiple wake model, therefore, provides a relationship to predict the nature of the shadowing and then determines the velocity along with the downstream distance of the wake. The velocity at a point is acquired by equating the deficiencies of kinetic energy in individual wakes of turbines with that of the interacting zones of the wake.

Larsen's wake model is also known as European Wind Turbine Standard II Model (EWTSII model) was developed by G.C. Larsen. This model can provide both first-order and second-order approximate solutions to the Prandtl turbulent boundary layer equations [16]. The model assumes incompressible, stationary, self-similar velocity profile and negligible wind shear of the atmosphere. The solution of the assumed axisymmetric flow provides the width of the wale and mean velocity along the downstream length of the wake [19]. Unlike, Jensen's wake model this model finds the rotor dimensions strongly affecting the wakes. However, for closely spaced wind turbines, this model gives smaller than actual values of Energy [17].

Frandsen model splits the wake into three sections and applies an internal boundary layer, within the planetary boundary layer, that is produced by the surface drag of the turbine [19]. The initial portion of the wake is considered where the wakes are not interacting yet. This section is followed by the interacting zones of the multiple wakes, where the only vertical expansion of the wake is assumed to occur. In the final part, the wake is considered in balance with the planetary boundary layer [20]. The mean wind speed over the rotor area is calculated by a semi linear method [21]. Therefore, the velocity deficit profile is 'hat shaped' just as predicted by Jensen's model. Compared with other analytical models, Frandsen's model predicts wider wakes and highest downstream wind velocities.

2.3.2 Field models

The scheme of modeling the wakes by any of the Field models is to solve the Reynolds-averaged Navier-Stokes equations with a separate model included for turbulence [19]. There are various codes available that have incorporated these models to simulate the flow through a wind farm or a portion of it. Two major types of field models are the Eddy viscosity model and three-dimensional field models.

Eddy viscosity model is applied to 2D domains only are therefore provides approximate but quick estimations of velocity and turbulence in the wakes. The main idea of this model is based on momentum shift into the wake zone from the flow surrounding it. Just like Jensen's model, this model also neglects the effects of the turbine on the atmospheric boundary layer. Hence these models neglect the wake losses in offshore arrays and not appropriate for studying offshore wind farms.

The models to solve the complete 3D flow through a wind farm are the most trending and accurate of all. These models mainly involve the parabolic shape of the Atmospheric boundary layer and the wake affected by ABL. Among many such models, the code developed by Energy Research Center by modifying the UPMWake model is prominent.

More recently the use of actuator disk, actuator line, and actuator surface modeling of the wind turbines has made it possible to simulate complete wind farms. These elliptic field models enable solvers like Ansys Fluent, OpenForm, and Ellipsys 3D to simulate the flows through wind farms. Such solvers are capable to include various turbulence models and boundary conditions as desired by the researchers. Hence, depending on the availability of computational resources, the computational fluid dynamic studies of wind farms are carried out to assess the wind turbine wakes. This thesis makes use of the actuator disk model to resolve the HAWTs of the FFCEL wind farm and then simulate the far wake for the existing configuration. Latter a vertically staggered orientation would be simulated to enhance power production. Thus, in the following section the Actuator Disk (AD) modeling would be revised.

2.3.3 Windfarm optimization

It is critical to address the optimization of the wind farm layouts to evaluate the problem at hand. An optimization problem generally has specific degrees of freedom from a range of variables to be catered to. It is otherwise almost impossible to optimize a configuration of wind turbines by considering all independent variables affecting the wind farm performance. The most widely applicable objective function of optimization of wind farms is to maximize power output [19]. The power production, however, is constraint by the number of wind turbines and their relative positioning.

Jensen's model is the most common method to optimize a finite wind farm for maximizing the energy output and minimizing cost. Both objectives could be met but it is carried out by increasing the distances among the turbines and hence installing a limited number of turbines. Such layouts are anyways expected to enhance efficiency but at the cost of under-utilizing the site area.

Summary

This chapter gives an overview of the research and relevant findings to date on the development of wind turbines and their utility on large scale. A special emphasis is given to the wind farm wake modeling techniques. The wake of a wind turbine can be identified as a near wake for the region up to 3D downstream of the rotor. Whereas the region beyond 3D is referred to as far wake. The two major groups of models utilized to study far wakes are categorized as kinematic models and field models. The kinematic models employ only the momentum equation to solve for velocity variations in the wake. However, the field models would solve for the turbulence by separately including a model for it. More importantly, any of these models can be solved analytically or numerically. Moreover, layout optimization of onshore wind farms is discussed with a particular focus on the vertical staggering of the wind turbines of a wind farm. It was concluded that the objective function of optimization requires enhancing a few parameters of the wind farm performance. Mostly, the wind farm layouts are optimized to increase the power output.

References

[1] "(No Title)." https://phys420.phas.ubc.ca/p420_16/lqliang/webpage.html (accessed Jan. 22, 2021).

[2] F. Castellani, D. Astolfi, M. Peppoloni, F. Natili, D. Buttà, and A. Hirschl, "Experimental Vibration Analysis of a Small Scale Vertical Wind Energy System for Residential Use," *Machines*, vol. 7, no. 2, p. 35, May 2019, DOI: 10.3390/machines7020035.

[3] "Betz limit - Energy Education." https://energyeducation.ca/encyclopedia/Betz_limit (accessed Dec. 23, 2020).

[4] "Advanced wake model for closely spaced turbines, AWEA 2005 - DNV GL." https://www.dnvgl.com/publications/advanced-wake-model-for-closely-spaced-turbines-awea-2005-98723 (accessed Dec. 28, 2020).

[5] "Status of wake and array loss research (Conference) | OSTI.GOV." https://www.osti.gov/biblio/6211976 (accessed Dec. 28, 2020).

[6] M. J. Churchfield Boulder, "A Review of Wind Turbine Wake Models and Future Directions (Presentation), NREL (National Renewable Energy Laboratory)," 2013.

[7] A. Crespo and J. Hernández, "Turbulence characteristics in wind-turbine wakes," *J. Wind Eng. Ind. Aerodyn.*, vol. 61, no. 1, pp. 71–85, Jun. 1996, doi: 10.1016/0167-6105(95)00033-X.

[8] S. P. Breton, J. Sumner, J. N. Sørensen, K. S. Hansen, S. Sarmast, and S. Ivanell, "A survey of modeling methods for high-fidelity wind farm simulations using large eddy simulation," *Philos. Trans. R. Soc. A Math. Phys. Eng. Sci.*, vol. 375, no. 2091, 2017, DOI: 10.1098/rsta.2016.0097.

[9] B. Roscher, R. Schelenz, A. Werkmeister, Y. Shkara, L. Stössel, and G. Jacobs, "Comparison of wind turbine loads inside a wake between engineering model and CFD calculation," in *Journal of Physics: Conference Series*, Jun. 2018, vol. 1037, no. 7, DOI: 10.1088/1742-6596/1037/7/072039.

[10] "(PDF) Aerodynamics of wind turbine wakes Literature review." https://www.researchgate.net/publication/242726502_Aerodynamics_of_wind_turbine_wakes_Literature_review (accessed Dec. 28, 2020).

[11] "Wind Energy Explained: Theory, Design and Application, 2nd Edition | Wiley." https://www.wiley.com/en-us/Wind+Energy+Explained%3A+Theory%2C+Design+and+Application%2C+2nd+Edition-p-9780470015001 (accessed Nov. 20, 2020).

[12] S. Frandsen *et al.*, "Analytical modeling of wind speed deficit in large offshore wind farms," in *Wind Energy*, Jan. 2006, vol. 9, no. 1–2, pp. 39–53, DOI: 10.1002/we.189.

[13] I. ; Katic, J. ; Højstrup, and N. O. Jensen, "A Simple Model for Cluster Efficiency," APA, 2021. Accessed: Dec. 28, 2020. [Online]. Available: https://orbit.dtu.dk/en/publications/a-simple-model-for-cluster-efficiency.

[14] Ainslie and J. F, "Calculating the flowfield in the wake of wind turbines," *J. Wind Eng. Ind. Aerodyn.;*, vol. 27:1–3, 1988.

[15] J. G. Schepers and S. P. Van Der Pijl, "Improved modeling of wake aerodynamics and assessment of new farm control strategies," *J. Phys. Conf. Ser. OPEN ACCESS*, DOI: 10.1088/1742-6596/75/1/012039.

[16] G. C. Larsen, "General rights A Simple Wake Calculation Procedure," Risø National Laboratory, 2021. Accessed: Dec. 28, 2020. [Online]. Available: https://orbit.dtu.dk/en/publications/a-simple-wake-calculation-procedure.

[17] T. Göçmen, P. Van Der Laan, P. E. Réthoré, A. P. Diaz, G. C. Larsen, and S. Ott, "Wind turbine wake models developed at the technical university of Denmark: A review," *Renewable and Sustainable Energy Reviews*, vol. 60. Elsevier Ltd, pp. 752–769, Jul. 01, 2016, DOI: 10.1016/j.rser.2016.01.113.

[18] D. J. Renkema, "Validation of wind turbine wake models Using wind farm data and wind tunnel measurements Douwe J. Renkema," 2007. Accessed: Dec. 28, 2020. [Online]. Available:

https://repository.tudelft.nl/islandora/object/uuid%3A0fbea4b9-990a-4d03-bb97-3474c4728d2f.

[19] J. F. Manwell, J. G. McGowan, and A. L. Rogers, *Wind Energy Explained*. Chichester, UK: John Wiley & Sons, Ltd, 2002.

[20] "Turbulence and turbulence-generated structural loading in wind turbine clusters (Thesis/Dissertation) | ETDEWEB." https://www.osti.gov/etdeweb/biblio/20685756 (accessed Dec. 28, 2020).

[21] "(PDF) Wake modeling for intermediate and large wind farms." https://www.researchgate.net/publication/229014374_Wake_modeling_for_intermediate_and_large_wind_farms (accessed Dec. 29, 2020).

Chapter 3

Wind farm numerical modeling methods

3.1 Rotor modeling

The CFD of wind turbines would require their complete geometries to simulate the flow through and around them. This demands Computer-Aided Design (CAD) models of the wind turbines and carrying out pre-processing for those models is a hectic and time-consuming part. Since the sizes of HAWTs used these days have become enormously large, thus generating a fine quality mesh for them requires extraordinary computational power. Given these challenges, it is almost non-practical to conduct the CFD of a complete wind farm by including the actual geometries of the wind turbines.

However, modeling the wind turbine geometries has developed the ease to simulate wind farm flows. In concept, these models replace the complex wind turbine geometry and include mathematical relationships that induce similar effects on the flow as that expected by the wind turbine. This allows reducing the complications of generating grids for turbines and reduces the computational load. It is indeed an approximate way of studying the flow but good enough to quickly predict the performance of both the wind turbines and the wind farms.

Some of the most common modeling techniques used to date involve the Actuator disk model (ADM), Actuator Line model (ALM), and the Actuator Surface model (ASM) [1]. Each of these methods is based on the principle of momentum conservation but their ability to imitate the actual flow behavior near the blades of a wind turbine and through it is different. The ADM and its implementation techniques in ANSYS Fluent would be addressed in detail. Whereas the other two models would also be briefly discussed in the following section.

3.1.1 Actuator disk model

As introduced above, the ADM is the simplest and quickest way of resolving the wind turbine geometry. Conceptually, it relies on the principle of momentum transfer [2]; where

a disc of zero thickness represents the turbine, and the forces on the turbine are calculated and uniformly distributed over the disc. In numerical setups, the permeable disc is constantly loaded, and the forces represent the turbine.

Many researchers have developed variants of the basic ADM to improve its ability to present the rotor's behavior in a flow-stream. Fundamentally, the ADM considers a stream tube of flow that extends both in upwind and downwind directions. A disc, representing the rotor, is placed at a point in the stream tube, such that it fits into the annulus of the stream tube. The flow velocity is assumed to be equal to the ambient velocity at stations far away on both sides of the disc. The physics of the flow in the stream tube is simply reflected by Bernoulli's theorem. Since the rotor extracts energy from the flow, thus the disc splits the flow stream into two segments. Bernoulli's theorem is separately applied to the flow on both sides of the disc. It is evident that due to the harvest of the kinetic energy of the flow by the rotor, the flow velocity would reduce behind the disc. Also, a sudden drop in the pressure would be caused. The actuator disc model thus relates the pressure drop caused by the turbine with the velocity deficit and hence creates a wake influenced by the operation of the rotor[3].

It is important to identify that the ADM does not account for the effects produced by the rotation of the rotor. The vortices that shed from the tips and the trailing edges of the turbine are also completely neglected. However, there are variants of ADM that combine with other approaches to fill for these flaws. The simple ADM generally considers the axial flow and neglects the radial flow. But the generalized actuator disc method modifies to include unsteady Navier-Stokes equations and thus removes any limits on the direction of flow.

Similarly, the ADM combines with Blade Element Theory (BET) to include the effects of localized flow behavior along the radial direction of the disc. BET considers portions of the disc such that each portion represents an annulus. BET requires tables of lift and drag coefficients of airfoils at respective radial positions. The aerodynamic forces are thus calculated for each annulus area on the disc, this gives a more accurate distribution of forces on the disc than that of ADM. When combined with momentum theory, BET develops into the Blade Element Momentum model (BEM) [4].

As described earlier, the generalized actuator disc model could depict the three-dimensional effects of the rotor. This model relies on BET to calculate the localized forces and then apply corrections to them. Altogether, the effects of the flows at the tips and radial sections are incorporated in this model.

The study of flow around a turbine or through a wind farm by using ADM requires both the modeling of the rotor by ADM and the flow around it is solved by applying Navier-Strokes Equations. The turbulence in the flow can be modeled by any suitable model for rotating bodies. Despite the modifications made to ADM; it is not suitable enough to study the near wakes of the wind turbines. However, it can be suitable for the far-wake studies of wind farms. As discussed in the previous chapter, ADM has been used by researchers to simulate the wind turbine wakes and their interactions. Based on those researches, this thesis would also utilize the ADM to study the wake effects on the downstream turbines of the FFCEL wind farm.

The mathematical modeling of flow through the actuator disk is based on the conservation laws of fluid dynamics. The simplest approach in this regard is to consider one-dimensional, incompressible, and steady-state flow through the disk. Further, a control volume like a stream tube around the turbine and extending to a large distance downstream is considered to apply the conservation laws. The integral form of conservation of mass for steady flow through the fixed and nondeforming control volume is given by the following equation.

$$\int_{cs} \rho V . \vec{n} dA = 0 \tag{1}$$

This equation reduces into a simple form if we assume no mass to enter and leave the boundaries of the stream tube. For three locations of our interest in the stream tube, namely the inlet, disk plan, and the outlet, the continuity equation is

$$v_1 A_1 = v_2 A_2 = v_3 A_3 \tag{2}$$

Where v_2 is the velocity on the disk plan and A_2 is the area of the disk. Likewise, v_1 and v_3 are velocities at inlet and outlet, respectively.

The conservation of linear momentum for steady flow through the stream tube is given in the integral form as,

$$\int_{cs} V\rho V.\vec{n}dA = \sum F_{cv} \tag{3}$$

For the assumptions stated above, this relationship reduces to the following analytical equation.

$$\rho v_3{}^2 A_3 - \rho v_1{}^2 A_1 = F_A \tag{4}$$

In this equation, F_A is the force exerted by the turbine to the flow due to a change in momentum of the flow upon passing through it. Finally, the conservation of energy through the stream tube containing the turbine is given below,

$$\int_{cs} (\breve{u}+\frac{p}{\rho}+\frac{V^2}{2}+gz)\rho V.\vec{n}dA = \dot{Q}_{net}+\dot{W}_{net} \tag{5}$$

Where $\breve{u}$ is the internal energy per unit mass, p is total pressure, g is gravitational constant, and z is the elevation. On the right-hand side, we have $\dot{Q}_{net}$ for the total heat per unit mass added to the system and $\dot{W}_{net}$ for the total work per unit mass done on the system. Since we have assumed an adiabatic system the right had side reduces to zero. The variations in internal energy and elevation can also be neglected to acquire Bernoulli's equation.

$$P_i+\frac{1}{2}\rho v_i^2 = \text{constant} \tag{6}$$

Since a wind turbine extracts energy from the flow, the energy equation cannot be applied to relate energies at points across the actuator disk. Thus, we apply Bernoulli's equation between the inlet and a point just ahead of the disk. Similarly, between a point just next to the disk and one located at the outlet of the stream tube. The equations obtained are given as,

$$P_1+\frac{1}{2}\rho v_1^2 = P_{f\cdot 2}+\frac{1}{2}\rho v_2^2 \tag{7}$$

$$P_3+\frac{1}{2}\rho v_3^2 = P_{b\cdot 2}+\frac{1}{2}\rho v_2^2 \tag{8}$$

The difference between these two equations gives the pressure difference across the actuator disk, where $P_{f.2}$ is the pressure in front of the disk and $P_{b.2}$ is the pressure just behind the disk.

$$p_{b\cdot 2}-p_{f\cdot 2} = \frac{1}{2}\rho v_1^2[1-\left(\frac{v_3}{v_1}\right)^2] \tag{9}$$

Multiplying this above equation with disk area gives the force exerted by the turbine on the flow.

$$F_A=(p_{b\cdot 2}-p_{f\cdot 2})A_2=\frac{1}{2}\rho A_2 v_1^2[1-\left(\frac{v_3}{v_1}\right)^2] \tag{10}$$

Comparison of this equation with the relationships for the conservation of mass and momentum derived earlier gives the following expression.

$$u_2=\frac{1}{2}(u_1+u_3) \tag{11}$$

This relationship of velocities on the inlet, disk, and outlet reveals that velocity at the rotor location is less than the incoming velocity. A more relevant parameter for the velocity field across a wind turbine is the axial induction factor, which is the ratio of velocity drop across the rotor and free stream velocity.

$$a=\frac{(u_1-u_2)}{u_1} \tag{12}$$

The power output and the efficiency of the turbine can be calculated in terms of axial induced factors by the equations stated below.

$$P=F_A u_2=\frac{1}{2}\rho A_2 v_1^3[4a(1-a)^2] \tag{13}$$

$$\eta=4a(1-a)^2 \tag{14}$$

The actuator disk model implement thus takes turbine efficiency and free stream velocity as inputs to solve for the pressure difference across the disk. Note that the power curves and experimental power production data for the turbines in the FFCEL wind farm are available.

3.1.2 Actuator Line Model

Actuator Line Model (ALM) is an enhancement of ADM. The principle of ALM's working is the same as that of ADM. But the ALM is completely a three-dimensional flow model that aims to include the finite number of blades and their effects on the flow[5]. ALM considers a line for each of the blades in a rotor of a wind turbine. The Line is split into a specific number of segments but unlike the BEM theory, there are points along the line for each portion of the blade. However, the approach of ALM is like that of BEM; to find the localized aerodynamic force from the respective airfoil data. Therefore, the ALM requires tabulated 2D-airfoil data to calculate the local angle of attack. Further, the lift and drag forces on the segments of the line are calculated as the function of the local angle of attack.

The rotational effects of the rotor are included in ALM by taking into account the angular velocity of the rotor. Since ALM relies on unsteady and incompressible Navier-Strokes Equations for the solution of the flows around the turbine. It is, therefore, more convenient to use ALM for the wake studies of Wind turbines. But the major concern is the implementation of ALM by using commercial CFD software is a very demanding task.

3.1.3 Actuator Surface Model

The Actuator Surface Model (ASM) is the most accurate and robust of all three actuator models. It closely resembles the ALM and builds on it to exclude some of the limitations of ALM. ALM provides the radial distribution of the forces on the blade of a rotor but fails to model the chord-wise flow behavior. This gap in the ALM is filled by ASM; it considers the virtual surfaces along the line representing the blade and gives the force distribution along the chord as well[6]. ASM does not require any physical surfaces to be made for its numerical implementation. Instead, it presents the distribution of difference of pressure along the chord of the blade at a given radial location. Thus, it requires the airfoil data on both the shape and aerodynamic coefficients to model the wind turbine rotor.

ASM is capable of best predicting the flow over the blades of a wind turbine. It might better present three-dimensional effects like root and tip vortices but still does not match the actual flow characteristics.

3.2 Implementation of actuator disc model in ANSYS Fluent

Actuator disc model can be solved both analytically and numerically for wind turbines but for wind farm wake studies it is more convenient to solve it numerically. Many researchers have developed add-In codes to model the rotors of the wind turbines by AD. Development and execution of such codes require both the understanding of the complete CFD problem and more importantly fine computer programming skills. Mostly the codes on ADM are in-house and specific to a problem. However, there are some ways of implementing this model in commercial software for CFD, like ANSYS Fluent. These methods are indeed a compromise on the accuracy of the results, but they have been commonly used in research for far-wake studies.

This thesis would also rely on two of such implementation methods of ADM, available in the ANSYS Fluent. The fan boundary condition in Fluent allows studying problems related to rotating fans. If observed closely, this boundary condition works like the ADM. The user must define an interior zone inside the mesh that is generated for the control volume around a real fan. The inputs to this boundary condition allow defining a pressure jump across the fan region that the actual fan might cause. Based on this pressure gradient, Fluent calculates a body force and adds it to the momentum equation. However, it is important to note that unlike a wind turbine, the fan is driven by the input of energy, and thus it generates the flow stream by suction. If the direction of the fan is reversed, which Fluent allows, the flow through and around the fan region would be like that of a wind turbine. This procedure has been used by some researchers and they find it suitable to study the far wake.

The other built-in boundary condition in ANSYS Fluent that can imitate an AD is the porous media boundary condition. In theory, porous media boundary condition allows simulated flows that include permeable membranes. Just like Fan boundary Condition, this BC also allows the definition of an interior region for the porous region and then applies a pressure difference across it. More importantly, the pressure difference across the defined region is based on Darcy's law. Which provides the pressure difference as a function of the velocity at the region defined, the thickness of the region, and the permeability of the zone[7]. If the efficiency of a turbine to be modeled by AD is known,

a relationship of the same order as that of the one used by porous media BC can be derived. This then helps find the pressure difference that the rotor of a wind turbine would create for the given flow conditions. This method has been used by few researches and found it suitable to study the far wakes only.

Thus, this thesis would implement the ADM for the turbines FFCEL wind farm by using both above-mentioned methods provided by ANSYS Fluent. The detailed implementation procedure would be presented in the next chapter.

3.3 Defining the numerical problem.

To conduct a CFD study it is recommended to define a comprehensive problem statement and then propose a step-by-step solution to it. Generally, a CFD problem is split into three major parts, pre-processing, Solution, and Post-Processing. The study starts with pre-processing, which contains the most important steps like generating a geometry, a mesh, and assigning boundary conditions. But the foremost and most important part is to define the problem. The solution part allows the user to pick the most suitable discretization schemes, flow properties, flow equations, and turbulence models, etc. Once a solution is acquired for the defined model, the results on various flow properties like velocity, pressure, and turbulence kinetic energy are tailored and presented in the post-processing phase.

3.3.1 Problem description

Here the problem at hand is described in a way that sets up well for the desirable solution. The wakes of two wind farms fall on the FFCEL wind farm, which is placed close to the upfront farms such that many of the wind turbines of FFCEL under-perform. The dominant wind direction is north-east and thus the Zorlu wind farm affects the FFCEL turbine the most.

The first part of the problem is to simulate the wakes of the Zorlu wind farm or get the data on the input velocities for the FFCEL wind turbines. In the second part of the problem, at least three rows of the most affected wind turbines of the FFCEL wind farm will be simulated for wake effects and performance in the existing layout. In the third part of the problem, a layout of the same turbines would be solved for the same conditions but

by varying the hub heights. At least two configurations of vertical staggering would be tested to acquire the suitable one; that produces more power than the current configuration.

Table 3.1: Technical specifications of the wind farms.

Factors	**FFCEL (Test Case)**	**Zorlu (Upstream)**		**TGF (Upstream)**
Operational Date	May 2013	July 2013		November 2014
Power Capacity (MW)	49.5	56.4		49.5
No. of Turbines	33 x 1.5MW	28 x 1.8MW	5 x 1.2MW	33 x 1.5MW
Turbine Make and Model	Nordex S77 1.5MW	Vestas V90 1.8MW	Vensys V62 1.2MW	Goldwind GW77 1.5MW
Hub Height (m)	80	80	69	85
Rotor Diameter (m)	77	90	62	77
Spacing	Irregular	Irregular		Irregular
Inter-Farm Minimum Distance (m)	-	~ 790		~ 1390

3.3.2 Flow equations and turbulence model

Although every step of a CFD study is worth a discussion but to describe the general outlook of the analyses, it is often convenient to mention the most important ones. As mentioned earlier, the solution of a fluid problem is governed by Navier-Strokes Equations. However, solving the actual form of these equations, even numerically, is not practically possible. Therefore, various simplified forms are derived by applying careful assumptions. There are three major ways of solving the flow equations for a CFD problem. The major pros and cons of these types are enlisted below.

Table 3.2: Description of the CFD modeling approaches.

Method	Approach of Solution	Strengths	Flaws
Direct Numerical Simulation (DNS)	It applies the exact Navier-Strokes equations to the flow.	The most accurate CFD method.	Computationally very expensive and time-consuming.
Large Eddy Simulation (LES)	It applies NS equations to regions of flow away from walls and models the flows near walls.	It is accurate to predict major flow features.	Computationally demanding for large domains.
Detached Eddy Simulation (DES)	It is like LES except that it applies the models from RANS to the flow at a sub-grid scale	Accurately predicts flow properties away from walls	The near-wall flow is not depicted well for the computational power it takes
Reynolds Average Navier-Strokes (RANS)	It models the complete flow stream.	Takes little computational power and time.	Least accurate of all the CFD problems

In this research, the Reynolds Average Navier-Strokes Simulation would be used to study the problem. It is important to realize that the simplified forms of flow equation compromise the detection of turbulence. Thus, various transport equations based on empirical constants are developed to assist the simplified NS equations to address some of the major turbulence properties.

The RANS equations do not solve for the flow variables by applying the actual flow equations. Instead, the flow variables are split into mean and fluctuating parts. Each flow variable is then calculated at the grid nodes by first taking time averages and then the

fluctuations about that mean are estimated. By decomposing the variables, RANS include more unknowns to the flow equations. These unknown expressions have the same units as that of stress, hence they are termed as Reynolds-Stresses.

These stresses require more equations to make a solvable set of relationships. This brings the need for turbulence models, which based on different assumptions relate the flow properties with the stresses to provide suitable transport equations. Therefore, in RANS there is a range of turbulence models to choose from. However, the choice of a turbulence model is based on the nature of the problem, computational resources, and the accuracy required for the solution. The turbulence models offered by RANS are given in the figure below and the selection of a model for this research would be discussed in the next chapter in detail.

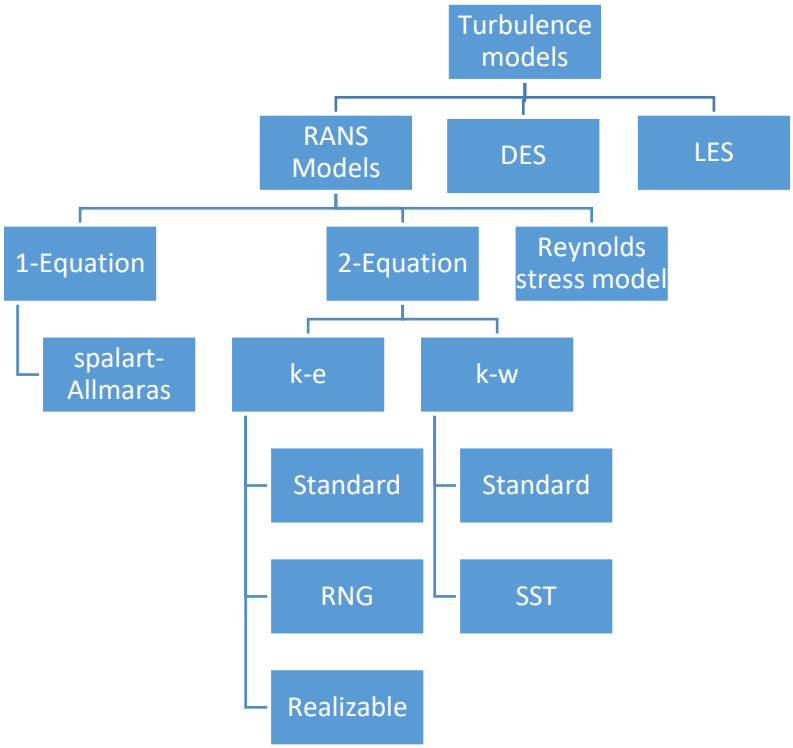

Figure 3.1: Flow chart of commonly used turbulence models.

3.3.3 Atmospheric boundary layer and wall functions

The Atmospheric layer over the earth's surface is itself a fluid flow problem. The vastness of the air layer involves both global and local events that make the ABL an interesting but complicated CFD problem. The wind shear over the surface is a constant phenomenon in the ABL but the convection of flows at various intervals of the day are more chaotic. Thus,

the flow in ABL should be addressed for its stability, temperature stratification, and indeed the ground effect.

With regards to stability, the ABL can be categorized as Neutral, Stable, and Unstable Atmosphere. The stability is determined as the tendency of the air in each locality to maintain at its initial conditions after it is subjected to a change. Since the consideration of the three types of ABL is not the objective of this research, thus convective atmosphere would be considered for the problem under study.

It has been noticed in the literature that the ABL has its turbulence sources, and the topology of a site plays a very vital role in the velocity and turbulence profiles. The roughness of the site would slow down the flow closer to the ground and any irregularities in the terrain on the site are a source of turbulence. Hence the modeling of the ABL involves various geometric parameters together with flow variables.

In numerical simulations the use of user-built velocity profiles to depict the ABL is common. However, the wall functions provided by ANSYS Fluent are also handy to generate a flow like that of in ABL. Generally, the wall functions take values for parameters to address the roughness of the terrain, but such models demand modifications to the values of the parameters to provide a more realistic representation of the ABL. Similarly, the values of the variables from the turbulence models also require carefully modified values to take the account of turbulence in the ABL. All specifications of all the matters mentioned above should be discussed in detail in the next chapter based on the models and approaches opted for the problem at hand.

Summary

This chapter presented a comprehensive insight into the methods and processes included to conduct this research. Primarily, the actuator disk model and its implementation in ANSYS Fluent 16.0, by using Fan Boundary condition and Porous media boundary condition, were discussed. Among the three actuator models, the actuator disk model was selected for its simplicity and low computational cost. The actuator disk model works on the principle of momentum loss across the rotor of the wind turbine. In more precise terms, the energy extracted by a wind turbine is modeled in terms of pressure and velocity drop. The porous media would allow creating a pressure jump across the rotor that is replaced with a porous disk. The flow behind the disk behaves more like that of a wake behind a wind turbine. The domain development and numerical setup with special emphasis on turbulence models are followed in the next section. Various numerical studies were consulted to arrange a suitable domain and setup for implementation of the numerical study through RANs. The k-e turbulence model was picked to model the turbulence and some modifications were made to ensure its compatibility with the problem setup. Finally, the wall functions and specific provisions made to model the Atmospheric Boundary Layer were presented.

References

[1] L. A. Martínez-Tossas, M. J. Churchfield, and S. Leonardi, "Large-eddy simulations of the flow past wind turbines: Actuator line and disk modeling," *Wind Energy*, vol. 18, no. 6, pp. 1047–1060, Jun. 2015, DOI: 10.1002/we.1747.

[2] J. D. Mirocha, B. Kosovic, M. L. Aitken, and J. K. Lundquist, "Implementation of a generalized actuator disk wind turbine model into the weather research and forecasting model for large-eddy simulation applications," in *Journal of Renewable and Sustainable Energy*, 2014, vol. 6, no. 1, DOI: 10.1063/1.4861061.

[3] T. Javaherchi, S. Antheaume, and A. Aliseda, "Hierarchical methodology for the numerical simulation of the flow field around and in the wake of horizontal axis wind turbines: Rotating reference frame, blade element method, and actuator disk model," *Wind Eng.*, vol. 38, no. 2, pp. 181–202, 2014, DOI: 10.1260/0309-524X.38.2.181.

[4] Z. Sun, J. Chen, W. Z. Shen, and W. J. Zhu, "Improved blade element momentum theory for wind turbine aerodynamic computations," *Renew. Energy*, vol. 96, pp. 824–831, Oct. 2016, DOI: 10.1016/j.renene.2016.05.035.

[5] P. K. Jha, M. J. Churchfield, P. J. Moriarty, and S. Schmitz, "Guidelines for volume force distributions within actuator line modeling of wind turbines on large-eddy simulation-type grids," *J. Sol. Energy Eng. Trans. ASME*, vol. 136, no. 3, pp. 1–11, 2014, DOI: 10.1115/1.4026252.

[6] X. Yang and F. Sotiropoulos, "A new class of actuator surface models for wind turbines," *Wind Energy*, vol. 21, no. 5, pp. 285–302, May 2018, DOI: 10.1002/we.2162.

[7] A. Manual, "Ansys Inc," *Canonsburg, PA*, vol. 15317, no. November, pp. 724–746, 2000, [Online]. Available: http://scholar.google.co.uk/scholar?hl=en&q=ansys&btnG=&as_sdt=1%2C5&as_sdtp=#7.

Chapter 4

Implementation of micro-scale CFD for FFCEL wind farm

4.1 Outline of the study

The methodology outlined for the study is presented in figure 4.1. The analysis involves various independent aspects of a wind farm study and therefore the input data to the final numerical model is separately processed in the pre-processing phase of the simulations. The fourth most important part was to acquire and process the wind data from the previously done WRF study to make Boundary Condition profile files of velocity and turbulence information. The second independent portion covered was to develop an algorithm to model the NORTEX 77m rotors as actuator disks. Based on simple momentum theory, the actuator disk model takes the turbine efficiency and incident velocity data as inputs to provide the pressure drop across the rotor. Further calculations were performed to identify specific constants required for the numerical implementation of this pressure and velocity jump across the disk in ANSYS FLUENT. In the third part, the separate analysis of a domain without wind turbines was done to simulate wind flows in both neutral and convective conditions of the atmospheric boundary layer. This pre-validated the implementation of the convictive conditions of ABL for a wind farm's CFD study. Finally, an appropriate mesh, including nine turbines from the FFCEL wind farm, was generated. The setup phase then acquired processed wind data, actuator disk parameters, and convective ABL conditions. Also, the ground roughness parameters and turbulence model constants were altered to meet the requirements of suitable ground roughness modeling and turbulence modeling of a real wind farm. Steady-state simulations were performed for average wind data of 1st and 2nd of July 2018. In the outputs of the simulations, we acquired velocity deficit plots, power variation plots, and wake interaction contours for each configuration of the selected turbines.

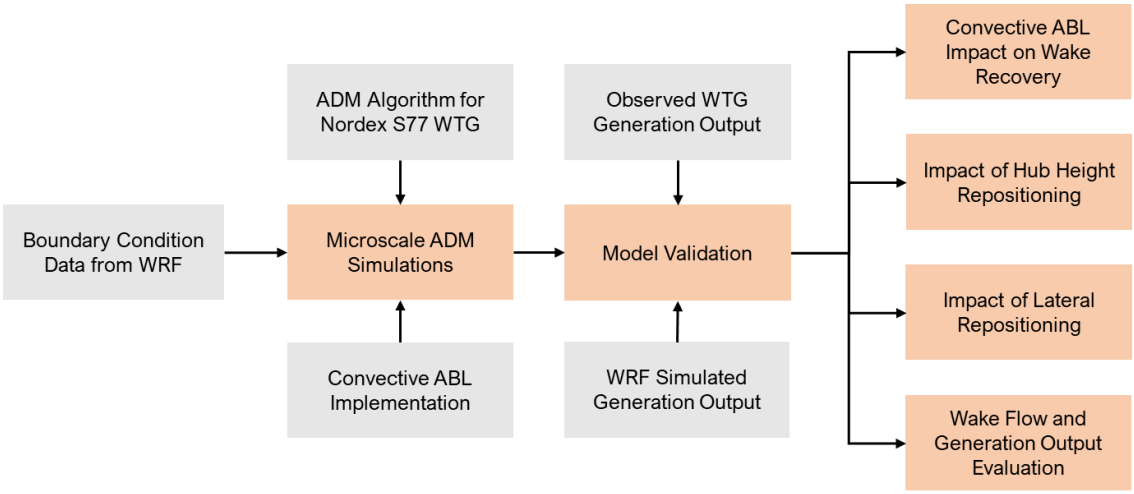

Figure 4.1: Methodology for numerical simulation of nine turbines of FFCEL wind farm.

4.2 Case study: Simulating nine turbines of FFCEL wind farm.

The parent WRF study simulated a domain covering three wind farms; ZORLU and TGF that are placed upfront of FFCEL in the direction of annual dominant wind direction. The WRF based mesoscale study identified turbines from the FFCEL wind farm that are most affected by the inter-farm wakes [1]. Hence, allowing us to pick the portion of the FFCEL farm that receives minimum velocity and highest turbulence from the compound wakes of ZORLU and TGF. To carry out a computationally affordable micro-scale CFD study, only nine turbines located in the southern part of the FFCEL wind farm were selected. The velocity field for the site and the selected wind turbines, enclosed in the white box are shown in Fig 4.2 (left). Note that T17 is outside of the selected zone; it is geographically located in the selected zone but the low spatially resolution of WRF has enforced its lateral shift. Fig 4.2 (top-right) shows the locations of all the turbines in the FFCEL wind farm. The selected 9 wind turbines include T21, T22, and T23 in the first row in the direction of the dominant wind, followed by T20, T27, and T28 in the second row. The third and last row has T17, T31, and T30.

4.2.1 Wind data processing

As highlighted in the background of this study, it is vital to acquire accurate inflow data to the CFD domain to analyze the effects of compound wakes from the upfront wind farms. In pursuit of this goal, the processing of the wind data is required to make it compatible with the CFD study. Since the wind direction for a site is an important

parameter to address as it changes with time and indeed the performance of the wind farm is affected by its variation. Including the variation of the wind direction in this study is again a demanding task and given that the FFCEL site receives most of its annual wind from one direction, as shown on the wind rose in Fig 4.2 (right bottom) [1], we opted for the dominant wind direction for all the simulations.

Generally, both experimental and WRF wind data are recorded at 10-minute intervals. Acquiring real-time wind data from WRF simulations of a site is an effective way of including incoming velocity and turbulence profiles in wind farm simulations. The WRF wind data has much lower spatial resolution than that of data from a micro-scale numerical study; on the order of several hundred meters [2]. Thus, it is critical to interpolate the WRF wind data to a much denser mesh of the CFD domain. Although, a complex and automated coupling of WRF and CFD is reported in the literature such approaches are themselves standalone research topics. For a quick analysis with limited computational resources, one might rely on the formatting of the most relevant wind data. Since ANSYS Fluent supports boundary condition profiles of a specific file format; we preferred to develop such files from the WRF wind data taken from the location surrounding the selected nine turbines.

The boundary condition profiles files were composed by including data for incoming velocity components, resultant velocities, and turbulent kinetic energy. Further, the coordinates of points in the CFD domain that corresponds to geographic locations of data points in the real wind farm, are also defined in the profiles. ANSYS fluent offers various interpolation schemes for different profile types. The most relevant profile type for 3D problems is mesh type, where the wind data defined for specific coordinates on the inlets are interpolated to each cell face on the boundary from the nearest data point [3]. The interpolation in fluent was appropriate to impose homogenous velocity and turbulent kinetic energy fields to the simulated domain, as required for correct CFD studies of problems including ABL [4].

The profile files for this case were written based on 27 data points taken from the WRF domain that correspond to equally spaced coordinate points on the inlets in the CFD domain. For steady simulations, the profiles contained average data of two days, 288-time intervals, for each field variable. We considered wind data of 1st and 2nd July 2018 as the observed data for the same days is also available, which provides reference data for the validation of simulated results. The proper replication of incoming wind flow to the CFD domain required appropriate boundary definitions too. The profiles and a specific domain setup, described in a section below, imitated close to the real flow field for the site.

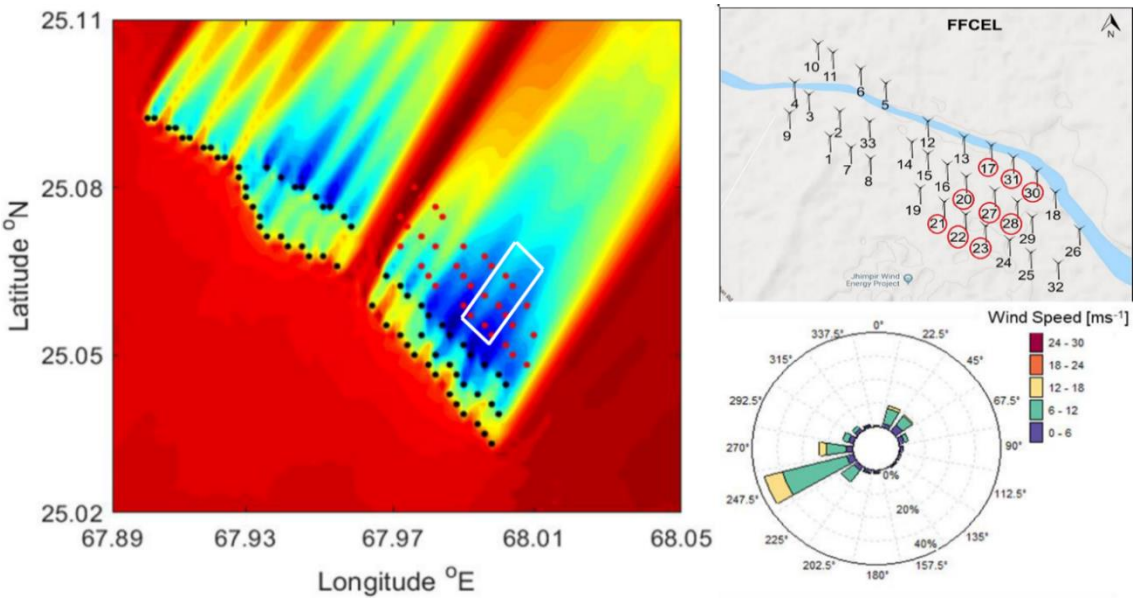

Figure 4.2: Wind farm layout: (left) Velocity contours of Zorlu, TGF, and FFCEL wind farms from WRF simulations, top view, (right-top) layout of FFCEL wind farm with selected turbines circled red, and (right bottom) wind rose for the site.

4.3 Numerical setup

Computational setup is of great importance to the approach used to simulate the wind farm under consideration. It is a challenging task to arrange a setup that is computationally affordable and still accurate enough to capture flow behavior on the scale desirable for a micro-scale study. Appropriate wind data input from WRF simulations required provisions to the domain shape, size, and boundary conditions. Hence consulting various research work on ABL modeling [4], WRF-CFD coupling methods [5] and micro-scale wind farm flow simulations involving ADM [6], [7],[8], the domain for the current study was designed.

4.3.1 Domain and boundary conditions

Figure 3 (left) shows the top view of the computational domain, where the turbines are shown in the current layout. The downstream arrangement of the turbines precisely imitates the existing wind farm. Fig 3 (right) shows the three turbines at 60m, 80m, and 100m hub heights. Although the turbines are located at 80m hub heights in the FFCEL wind field, the arrays are hypothetically placed at 60m and 100m to present the concept of vertical staggering for same sized rotors at different hub heights. The dimensions of the control volume captured by the grid are 1067x250x2100 along the X, Y, and Z-axis, respectively. The domain has nine cylindrical volume domains of 77m diameter and only 0.5m thickness, one for each turbine. The boundary conditions were applied to both the surfaces of the outer domain and the interior type of actuator disk zones. The cylindrical disks were defined as porous media. Each porous disk was supplied with the values of parameters that would create the pressure and velocity jumps based on the calculations from the Actuator disk theory explained previously. There a three velocity-inlet surfaces on the outer domain. As of the typical CFD approaches, the face in front of the first row of wind turbines is the first velocity inlet. The other two are the left and right surfaces in the YZ plane of the domain. The bottom face is defined as the wall section with specific parameters of roughness defined to imitate the roughness of the ground at the site. The rear and the opposite surface of the first inlet is the outlet of the domain with a 100% outflow fraction applied to it. Lastly, the top of the domain is given a symmetric boundary condition.

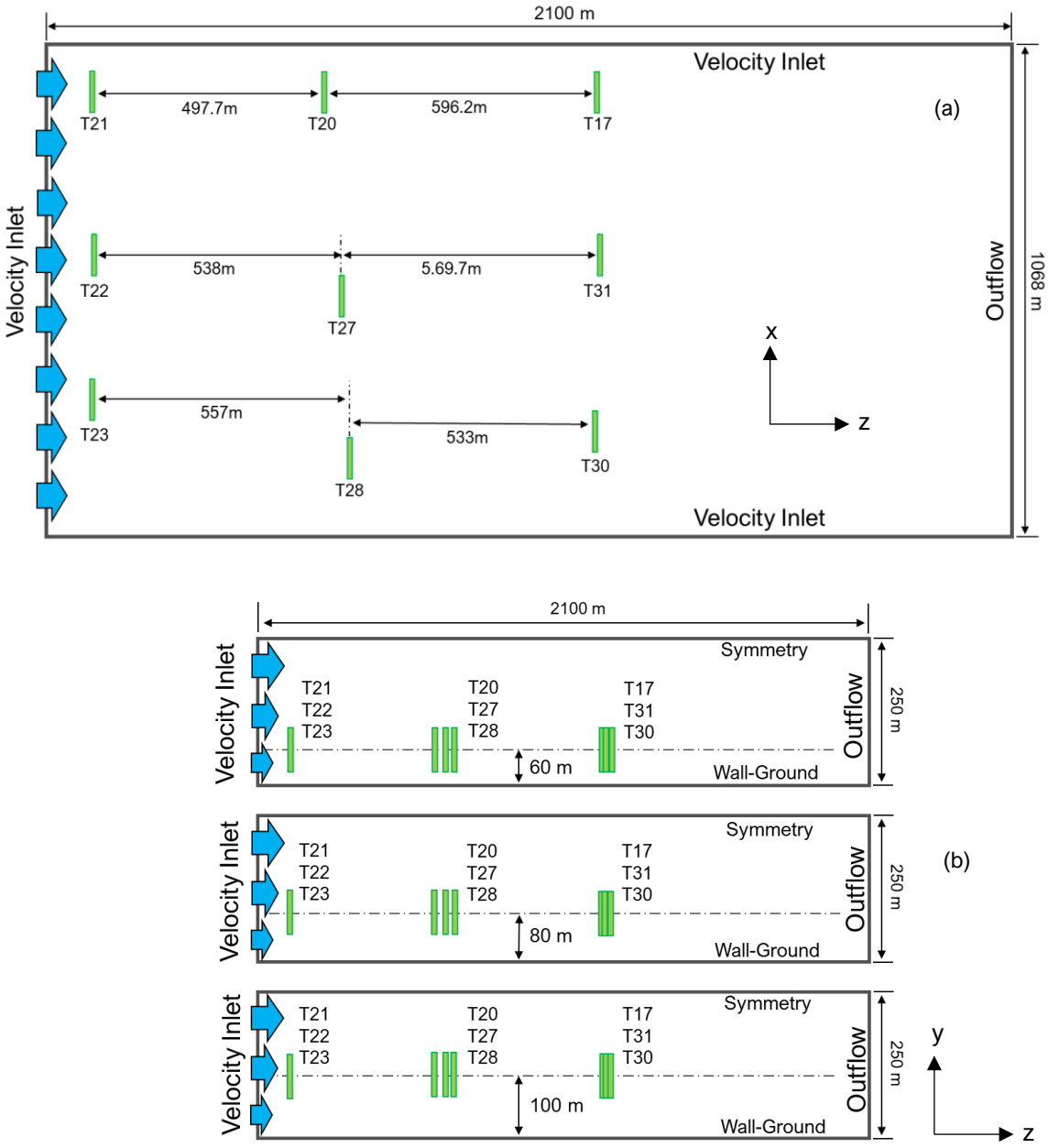

Figure 4.3: (a) Top view of domain: Actuator disks labeled green, and (b) side view of domains representing turbines at 60m, 80m, and 100m.

4.3.2 The grid and grid independence study

The grid sensitivity study was carried out by developing four meshes of different sizes. As shown in Fig 4.4 (left), the mesh was kept finer near the ground and adjacent to the actuator disks to capture the flow behavior on a reasonably smaller scale. Fig 4.4 (right) illustrates the variation of mean velocity at 100 meters; for the case where the rotors are also placed at this height. It can be seen from the plot that for denser meshes the mean

velocity increases. But for mesh sizes above 8.5 million cells, there is no significant hike in the mean velocity for converged solutions. Meshes denser than 12 million cells showed much smoother velocity deficit plots but the trend for cell counts beyond 8.5 million were the same. Therefore, it was reasonable to tradeoff smoother velocity deficit profiles for affordable smaller mesh sizes. Hence all the solved meshes were in the range of 9 million to 13 million and could still capture the velocity deficit downstream of the rotors to a degree that a much denser grid would do.

The maximum cell size in the zones for the actuator disks is 0.3m and the regions around the disks have cell sizes on the scale of 0.3m and growing into larger cells away from the disks. An outer rectangular domain capsules all the actuator disks. The mesh on each surface of the outer domain is finer at the edges to allow a more accurate distribution of wind data imposed to the inlets and further to allow smoother interpolations. The maximum cell size allowed in the outer domain is 40m, which are mostly located in the middle portions of the surfaces and indeed considerably away from each actuator disk. The mesh in normal to the ground surface of the outer domain was also made finer to allow to capture the turbulent eddies of small scale near walls. Although, the vertical heights of cells adjacent to the ground should be on a scale of less than a meter, [4] the roughness modeling of the ground hinders much smaller cell heights [9]. Therefore, the first cell height was kept at 0.5m which grows with a scale factor of 1.2 in the vertical direction; these provisions to the mesh are required to model the ABL [4]. Altogether, the grids for the simulated cases had a cell count in the range of 9 to 13 million.

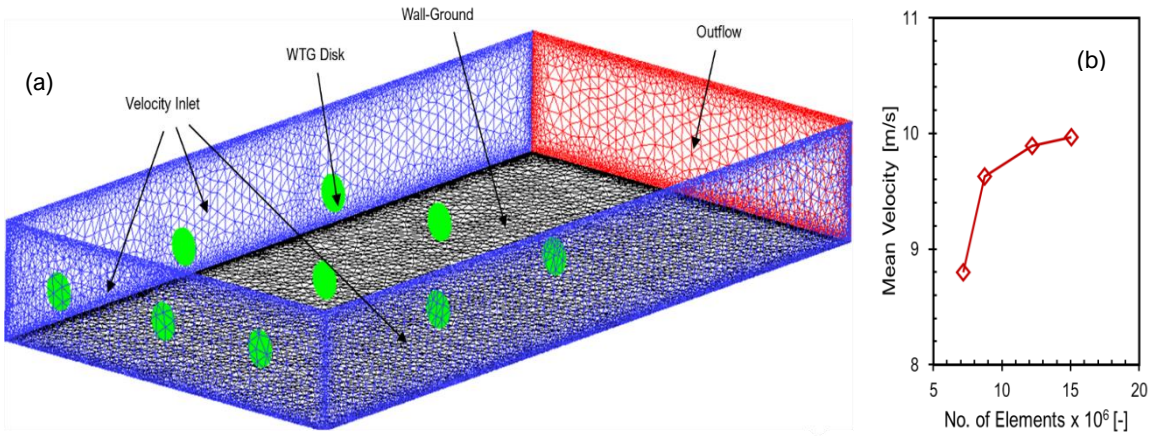

Figure 4.4: Computational grid: (a) grid and boundary conditions, and (b) grid independence analysis with mean wind velocity variation at 100 m hub height with respect to mesh density.

4.3.3 Solver setup

The numerical setup for the problem at hand required various adjustments to the models used for modeling convective atmospheric boundary layer, turbulence, and ground roughness. The pressure-based solver opted over the density-based solver as the flow regime is incompressible. A standard k-ε model with standard wall functions was used to model the turbulence. The energy equation was employed to solve the temperature stratification phenomenon in the ABL. A coupled pressure-velocity coupling scheme along with second-order upwind discretization for all other field variables was applied. Integrated velocity values on inlet surfaces and the outlet were monitored to decide the convergence of the solution. It was observed that for residuals below 1e-03 the surface velocity integrals were constant on both surfaces. However, the iterations were terminated for continuity residual dropping below 1e-04 and that of for the other variables below 1e-06. The detailed solver settings made for convective ABL, turbulence, and ground roughness is discussed below.

4.4 Convective atmospheric boundary layer modeling

The stability of the Atmospheric Boundary Layer is generally categorized into neutral, stable, and unstable states. It is much easier to simulate neutral or stable ABL than that of unstable ABL. It is because for the earlier two states of ABL the variations in many of the parameters governing the state of ABL are not considered. Of the several important parameters to address for a well-defined simulation problem involving unstable ABL, the buoyancy effect due to surface heat flux is the most prominent factor. Usually, temperature stratification is caused by heat flux from the ground to the adjacent layers of air. The warmer air flows into the higher layers of ABL and hence causes vertical momentum flux which might be beneficial to wake recovery [10]. For a site similar to a desert with no vegetation, like that of the FFCEL wind farm, the buoyancy affects the flow significantly during hot sunny hours [11]. Based on the above-mentioned facts, the study of the buoyancy effect due to ground heat flux to wind farm flow is modeled in ANSYS Fluent by using the Buoyancy model and some further definitions of the setup. Firstly, gravity is enabled and operational temperature under the Boussinesq parameters is defined based on the section of the day. The full buoyancy effects for turbulence

modeling are also included in the setup. For the velocity-inlet boundary conditions, the temperatures matching the operating conditions are defined for the thermal tabs. The density of the air is then defined as Boussinesq, where appropriate values for density and thermal exponential coefficient are defined. Finally, the heat flux from the ground is defined, which assumed values for a sunny day. These parameters are shown in table 4.1.

Table 4.3: ADM model parameters.

Convective ABL	
Operating Temperature	300 K
Air Density	1.205 kg/m^3
Heat Flux	250 W/m^2
Thermal Expansion Coefficient	0.00343 1/K
Modified k-ε model parameters	
C_μ	0.03329 (default 0.09)
$C_{1\varepsilon}$	1.176 (default 1.44)
Ground roughness	
Roughness Class	1
Roughness Constant	0.5
Roughness Length	0.03 m

4.5 Ground roughness and turbulence modeling

Ideally, the site topology of a wind farm should be included to wind energy numerical study by developing computer-aided designs that would closely replicate the ground roughness of the site. However, for a study constraint by the computational power and time, the roughness can be modeled by appropriately defining roughness constant and roughness height. In ANSYS Fluent the ground roughness is defined based on pipe flows and sand grain roughness. Further, the sites are generally classified and roughness constants are defined for each type of site [12]. Thus, modifications to the roughness parameters are required to attain a reasonable ground roughness to include the structure of the incoming flow. As prescribed in the literature, the no-slip condition was applied to the wall representing the ground. The roughness height of 0.6m and roughness constant of 0.327 was used to model the ground roughness [9].

The use of high fidelity numerical models, such as large-eddy simulations (LES), is desirable to study real wind farm wakes [13]. However, dense meshes and increased computational time are the penalties incurred for opting for models like LES. On the other hand, the Reynolds Average Navier-strokes (RANS) method of modeling turbulence offers the opportunity to simulate turbulence with coarser meshes and lesser computational time. RANS cannot solve turbulence and especially eddies on smaller scales, those close to the walls, rather applies mathematical models to capture the turbulence behavior [14]. RANS have various turbulence models that are specific to various flow types. For flows through wind arrays and wind turbines, the k-w and k-e models are often used [15], [16]. Taking into view the unstable ABL modeling, a modified standard k-e model was implemented for this study. Although, literature has reported the k-e model to underestimate velocity deficit behind an actuator disk [17] the modifications to the model for enhanced accuracy and suitability to ABL studies are already executed [18]. For this study, we preferred to adopt the modified k-e standard model developed by Matias Avila [18]. This model alters the coefficients of the k-e model and includes the effects of Coriolis, which is vital to the structure of ABL and wake recovery. However, the Coriolis effects are not included in this investigation as the height of the domain is small to cater to the large-scale flows.

Summary

This chapter described the implementation of a micro-scale numerical study of the FFCEL wind farm by manually coupling the CFD model with a WRF based mesoscale numerical study already performed for the site. The initial part of the chapter introduced the case study and pre-processing of the wind data acquired from the WRF study. The numerical setup for the micro-scale study is described in the middle section of the chapter and towards the end, the modeling of ABL, ground roughness, and turbulence are discussed.

References

[1] A. H. Syed, A. Javed, R. M. Asim Feroz, and R. Calhoun, “Partial repowering analysis of a wind farm by turbine hub height variation to mitigate neighboring wind farm wake interference using mesoscale simulations,” *Appl. Energy*, vol. 268, p. 115050, Jun. 2020, DOI: 10.1016/j.apenergy.2020.115050.

[2] R. Yuan *et al.*, “Coupled wind farm parameterization with a mesoscale model for simulations of an onshore wind farm,” *Appl. Energy*, vol. 206, pp. 113–125, Nov. 2017, DOI: 10.1016/j.apenergy.2017.08.018.

[3] “ANSYS FLUENT 12.0 User’s Guide - 7.6.3 Using Profiles.” https://www.afs.enea.it/project/neptunius/docs/fluent/html/ug/node266.htm (accessed Nov. 20, 2020).

[4] B. Blocken, T. Stathopoulos, and J. Carmeliet, “CFD simulation of the atmospheric boundary layer: wall function problems,” *Atmos. Environ.*, vol. 41, no. 2, pp. 238–252, Jan. 2007, doi: 10.1016/j.atmosenv.2006.08.019.

[5] P. Durán, C. Meißner, K. Rutledge, R. Fonseca, J. Martin-Torres, and M. S. Adaramola, “Meso-microscale coupling for wind resource assessment using averaged atmospheric stability conditions,” *Meteorol. Zeitschrift*, vol. 28, no. 4, pp. 273–291, 2019, DOI: 10.1127/Metz/2019/0937.

[6] A. Avramenko, O. Agafonova, J. Sorvari, H. Haario, and Y. Avramenko, “Fast numerical modeling method for wind flow investigation based on depth-averaged equations,” in *WIT Transactions on Engineering Sciences*, 2017, vol. 118, pp. 21–29, DOI: 10.2495/CMEM170031.

[7] K. S. Hansen *et al.*, “Simulation of wake effects between two wind farms,” in *Journal of Physics: Conference Series*, Jun. 2015, vol. 625, no. 1, DOI: 10.1088/1742-6596/625/1/012008.

[8] S. Aubrun, S. Loyer, P. E. Hancock, and P. Hayden, “Wind turbine wake properties : Comparison between a non-rotating simplified wind turbine model and a rotating model.”

[9] J. Franke *et al.*, “Recommendations on the use of CFD in wind engineering.” p. C.1.1-C1.11, 2004, Accessed: Nov. 20, 2020. [Online]. Available: https://research.tue.nl/en/publications/recommendations-on-the-use-of-cfd-in-wind-

engineering.

[10] S. Xie, C. L. Archer, N. Ghaisas, and C. Meneveau, “Benefits of collocating vertical-axis and horizontal-axis wind turbines in large wind farms,” *Wind Energy*, vol. 20, no. 1, pp. 45–62, Jan. 2017, DOI: 10.1002/we.1990.

[11] Y. Ao, J. Li, Z. Li, S. Lyu, C. Jiang, and M. Wang, “Relation between the atmospheric boundary layer and impact factors under severe surface thermal conditions,” *Adv. Meteorol.*, vol. 2017, 2017, DOI: 10.1155/2017/8352461.

[12] J. Wieringa, “Updating the Davenport roughness classification,” 1992.

[13] Y. Wang, W. Miao, Q. Ding, C. Li, and B. Xiang, “Numerical investigations on control strategies of wake deviation for large wind turbines in an offshore wind farm,” *Ocean Eng.*, vol. 173, pp. 794–801, Feb. 2019, DOI: 10.1016/j.oceaneng.2019.01.042.

[14] M. Balogh, A. Parente, and C. Benocci, “RANS simulation of ABL flow over complex terrains applying an Enhanced k-ε model and wall function formulation: Implementation and comparison for fluent and OpenFOAM,” *J. Wind Eng. Ind. Aerodyn.*, vol. 104–106, pp. 360–368, May 2012, DOI: 10.1016/j.jweia.2012.02.023.

[15] A. Bechmann, N. N. Sørensen, J. Berg, J. Mann, and P. E. Réthoré, “The Bolund Experiment, Part II: Blind Comparison of Microscale Flow Models,” *Boundary-Layer Meteorol.*, vol. 141, no. 2, pp. 245–271, Nov. 2011, DOI: 10.1007/s10546-011-9637-x.

[16] F. A. Castro, J. M. L. M. Palma, and A. S. Lopes, “Simulation of the askervein flow. Part 1: Reynolds averaged Navier-stokes equations (k - ε turbulence model),” *Boundary-Layer Meteorol.*, vol. 107, no. 3, pp. 501–530, Jun. 2003, DOI: 10.1023/A:1022818327584.

[17] X. Liu *et al.*, “Conference Series PAPER • OPEN ACCESS To cite this article: Matias Avila et al,” *J. Phys.*, vol. 854, p. 12002, 2017, DOI: 10.1088/1742-6596/854/1/012002.

[18] M. Avila, A. Gargallo-Peiró, and A. Folch, “A CFD framework for offshore and onshore wind farm simulation,” in *Journal of Physics: Conference Series*, Jun. 2017, vol. 854, no. 1, DOI: 10.1088/1742-6596/854/1/012002.

Chapter 5

Results and discussion

5.1 Validation of the numerical model

The power output characteristics of both CFD and WRF models are plotted in Fig 5.1 along with the observed powers for the selected turbines. The powers predicted by CFD simulations are much closer to observed powers than that of WRF's predicted powers. This establishes the superiority of micro-scale numerical simulations for their improved accuracy than that of mesoscale numerical studies. To further understand the power patterns of individual turbines, the differences of powers from both CFD and WRF studies are compared with observed powers. As demonstrated on the radar chart in Fig 5.1, WRF significantly underestimates the velocities in the wakes of turbines. In the case of the CFD study, the powers of turbines in direct wakes of upfront turbines are underestimated.

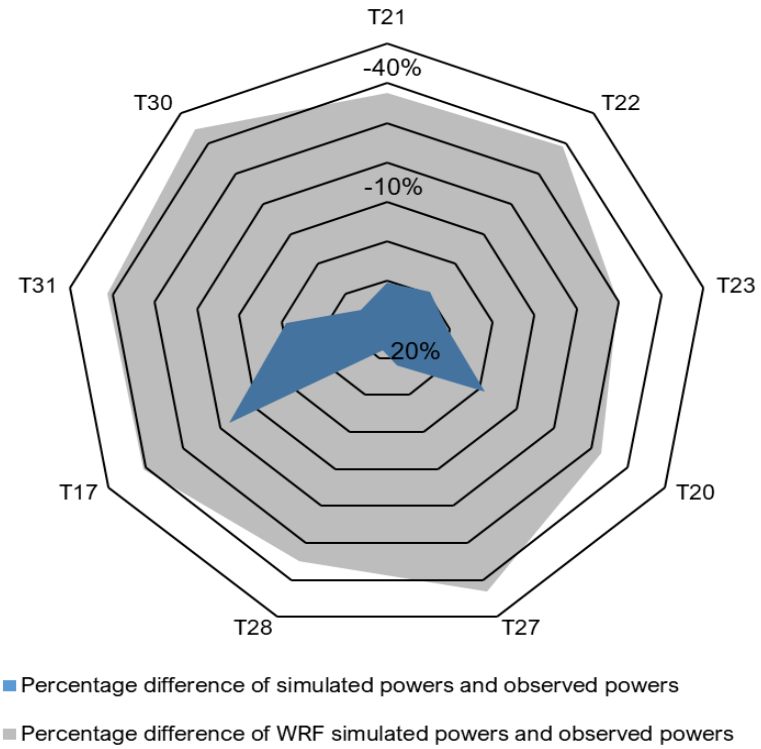

Figure 5.1: Comparison of observed powers with powers calculated from CFD and WRF simulations.

Whereas, for the rest of the turbines the powers are slightly over predicted. Nonetheless,

the percentage difference of observed and CFD powers is in the range of 0 % to 22 %. Whereas the difference between observed and WRF powers is in the range of 30 % to 45 %. CFD simulations prove enhanced accuracy over the WRF scheme. Also, the difference of CFD results to observed ones is in an acceptable range to proceed with the method for adoption as a quick tool to applied wind farm wake studies.

5.2 Comparison of velocity deficit plots for neutral and convective ABL

Velocity deficit profile along the length of the entire domain at 80 m height and passing through the center of the actuator disk for T30 is given in Fig 5.2. The comparison of Fig 5.2 (left) and (right) reveals quicker recovery of wake in case of convective ABL. The velocity at locations -2000 m for turbines at 100 m hub heights appears to reach 10.1 m/s for C-ABL, which is 0.3 m/s higher than that of N-ABL. Likewise, for turbines at 80m hub heights, the velocity has recovered to 9.2 m/s for C-ABL and only 8.8 m/s for N-ABL. However, for the case where turbines are at 60 m hub heights, the velocity recovery appears slightly higher in the case of C-ABL. Since in convective ABL the heat flux from the ground causes the vertical flux of velocities that assists in quick recovery of the velocity loss. The turbulence is expected to increase due to up gusts caused by the convection of warm air bodies to higher levels. This should prove beneficial for the recovery of the velocity drops, but this model shows slightly higher velocity recovery for convective ABL than that of the neutral ABL.

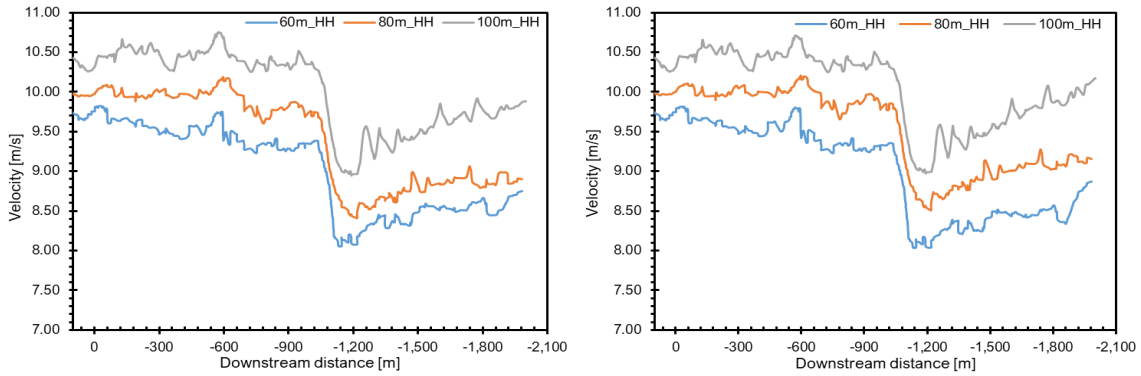

Figure 5.2: (left) velocity deficit plots for T30 at 60 m, 80 m and 100 m hub heights for neutral ABL, and (right) velocity deficit plots for T30 at 60 m, 80 m and 100 m hub heights for convective ABL.

5.3 Wake recovery and interactions

Figure 5.3 shows velocity recovery plots at various downstream locations for each turbine at 80m hub height. Since the turbines of the FFCEL wind farm are arranged in three rows in the direction of the main wind speed. The nine turbines of our consideration have T21, T22, and T23 in the first row and their respective lateral locations are -349.6 m, 0 m, and 323 m in the domain. In row two the turbines T20, T27, and T28 are positioned at lateral locations of -349.6 m, 87 m, and 451 m, respectively. Whereas in the third row, T17, T31, and T30 are installed at lateral spots of -349.6 m, 0 m, and 393 m, respectively. The lateral positioning reveals that T21, T20, and T17 are aligned and T22 is aligned with T31 of the third row. The velocity plots show velocity values in the range of 9.4 m/s to 9.6 m/s on the velocity inlet at lateral location -445 m. Whereas, on the opposite velocity inlet at lateral location 623 m, the values for velocity values are in the range of 8.45 m/s to 8.65 m/s. This variation of velocity on the velocity inlets at various downstream positions is due to the customized data from WRF results for the effects of wakes imposed on the CFD domain.

The lateral distribution of wind speed at locations 1.5D and 5.5D are arranged row-wise corresponding to velocity contours of respective turbines in vertical plans at the same downstream locations. The cone-shaped velocity curve behind T21 shows the wake to recover up to 8.6 m/s. Whereas, for T22 and T23 the velocity recovery is slightly higher as the velocity reaches 8.7 m/s. It can be seen in the velocity fields at 1.5D that more than half of the rotor appears blue and only the portions above the half-line show a gradual increase in the velocities until it reaches about 10m/s at the upper edge of the rotor. At 5.5D location the velocity recovers to 9m/s for T21, 9.2 m/s for T22 is 9.2 m/s and increases to 9.1 m/s for T23. Velocity distribution in the vertical plan at this location indicates the color bands to translate downwards into the rotor annulus area. This is the indication of significant recovery of the velocity behind the rotors compared with that of at 1.5D locations. It was also observed that velocities outside of the wakes of the turbines fluctuate in the range of 9.9 m/s to 10.2 m/s. These higher velocities in regions away from the wakes infer that the lateral distancing of first row turbines is high enough to allow the

diffusion of flows laterally. Also, the variation in velocity for regions outside of the wakes indicates the existence of the effects of compound wakes from the upfront wind farms.

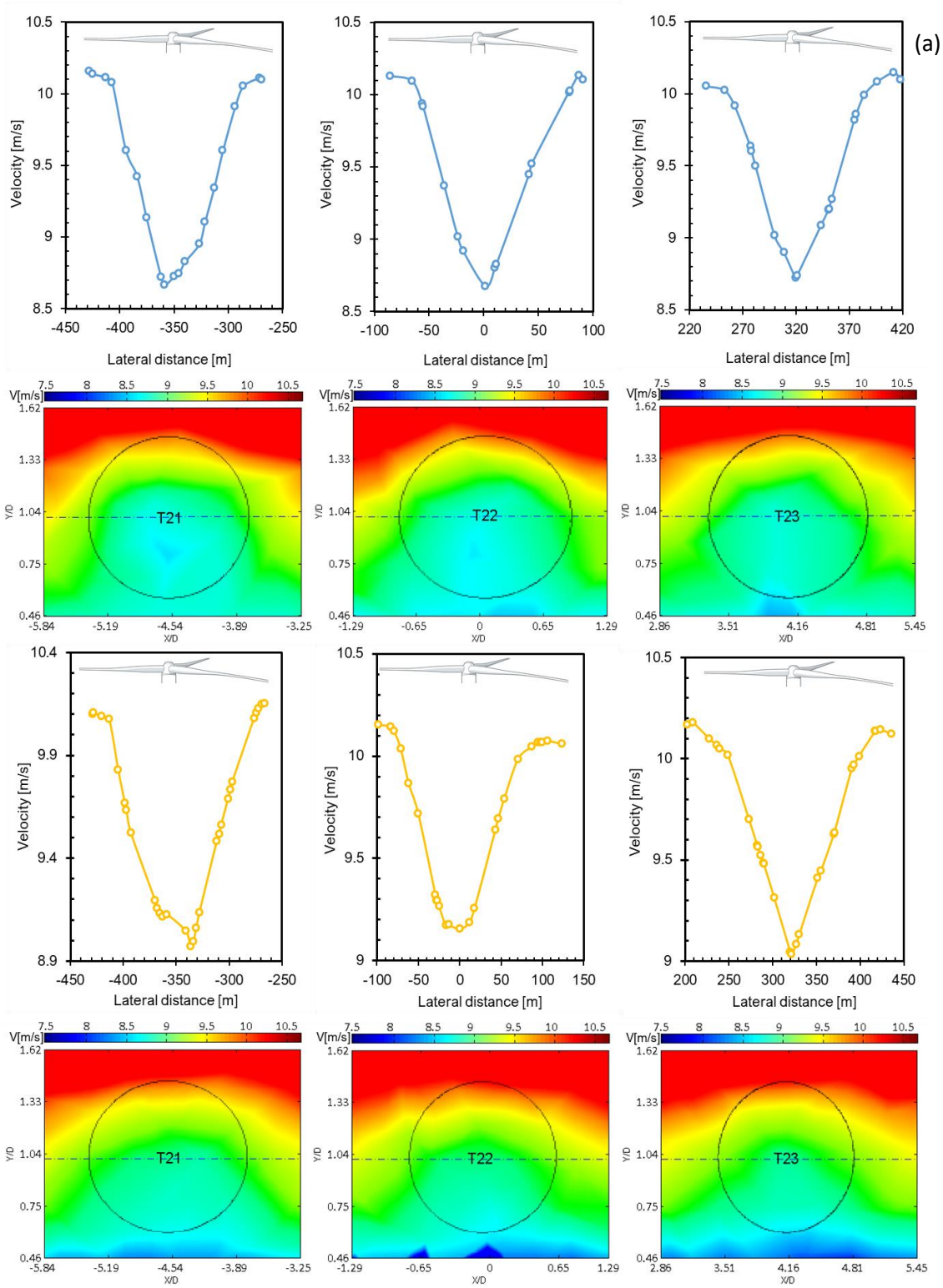

Figure 5.3: (a) velocity recovery plots against lateral length of the CFD domain at downstream locations 1.5D (blue) and 5.5D (orange) of T21, T22 and T23.

The turbines in the second row give an insight into both the interaction of the intra-turbine wakes and velocity recovery profiles. As shown in Fig 5.3 (b), the wake behind T20 seems to recover to 8.2 m/s at a 1.5D downstream distance. This is significantly lower than that of velocity recovery for T21 for the same downstream distance. This reveals the impact of the velocity deficit caused by T21 on T20. The curve presenting the velocity profiles for T27 at 1.5D shows a broader lateral spread and an indent at a lateral location of 0m. This is the effect of the wake of T22, which appears to mix with the wake of T27. Two troughs can be seen behind T28, where velocity spreads from 200 m to 500 m laterally. Since T28 is 128 m away from T23 in the lateral direction, thus the wake of T23 slightly overlaps with that of T28. At around 400m the spike corresponding to 10.1 m/s is shorter than any other spikes on the graph; this is where the wakes combine for T23 and T28. The velocity contours at the 1.5D location for the turbines in the second row endorse the findings for velocity recovery. The doomed-shaped color bands of blue, yellow, and orange validate the velocity deficits caused by the rotors. The excessive blue shading is the reflection of mild velocity gains to this point behind each turbine. Further, the sheared vertical distribution of velocities corresponding to the areas of the rotors in the representation of ABL's interaction with the wakes of the turbine. As we proceed to the plans at 6.6D behind each of the second rows of turbines, the damping of the velocity curves becomes obvious from the plots. The minimum velocity is 8.5 m/s in the wake of T20 and for T27 and T28 the wake has recovered to 9.3 m/s and 9.15 m/s, respectively. The higher velocity recovery for T27 and T28 is because of their lateral misalignment with that of the upfront wind turbines. The mixing of the wakes is also clear as the indent at 0 m has almost vanished and that of the spike at 400 m has become shorter than that at 1.5D. The velocity field for each turbine demonstrates enhanced velocities. The flatting of color bands and the diffusion of higher velocity bands into lower parts of the rotor annulus is evidence of increased velocities by 6.5D locations.

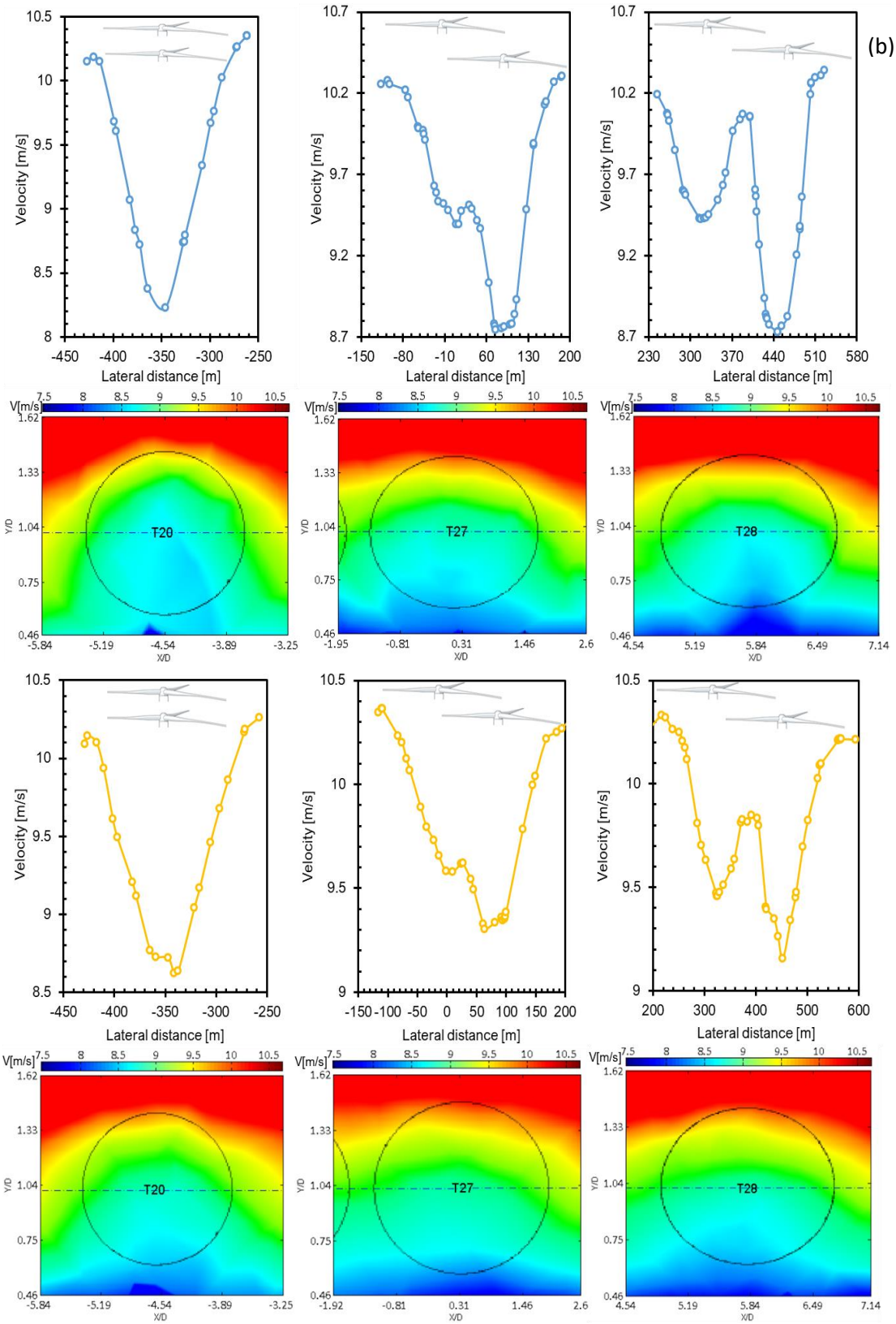

Figure 5.3: (b) velocity recovery plots and contours against lateral length of the CFD domain at downstream locations 1.5D (blue) and 6.5D (orange) of T20, T27 and T28.

Lastly, Fig 5.3 (c) shows the wake recovery of the turbines in the third row of the domain. As expected, these turbines receive the least of the velocity flowing into the domain because they receive diminished flows from the upfront rows of the turbines. Since T17 operates right behind T21 and T20, the shape of velocity deficit curves for these three turbines is perfectly the same. However, the velocity drops behind T17 is higher as it plunges to 7.8 m/s at 1.5D downstream location. Whereas, for T31 and T30 the velocity recovers to 8.6 m/s by 1.5D downstream locations behind them. The wider plot area behind T30 and T31 shows the fused wakes and the slight diversion at location 90 m also complements the wake mixing of T31 and T27. However, the wakes of both T27 and T28 appear to overlap that of T30, this is evident from deflections of the curve behind T30 at 350 m and 460 m. The velocity contours for 1.5D locations of these turbines show the overlapping rotor areas of T23, T30, and T28; further, T27 shares a significant portion with T31 towards its left side. The rotor area of T17 is mostly dark blue, which indicates the least velocity received by T17 compared with any other turbine. Moreover. T31 is partially influenced by the wake of T27, where the contours are inclined from the center of T31 to T27. The wake of T28 affects T30 more than that of T23 because it is more than a kilometer upfront of T30. The slope of contour lines is greater from the center of T30 to T23 than those from T30 to T28 towards the right side. The plots for locations 6.5D of these turbines claim velocity recovery to a minimum of 8.4 m/s behind T17 and that of for T31 to 9.3 m/s. T30 also receives a hike to 8.95 m/s from 8.6 m/s at the 1.5D location. The visualization of velocity distribution on the vertical plans at 6.5D locations validates the velocity hikes across the areas corresponding to the rotor. The flatting of color bands and diffusion of dark blue into cyan color towards the bottom of the rotor is evidence of the wake recovery.

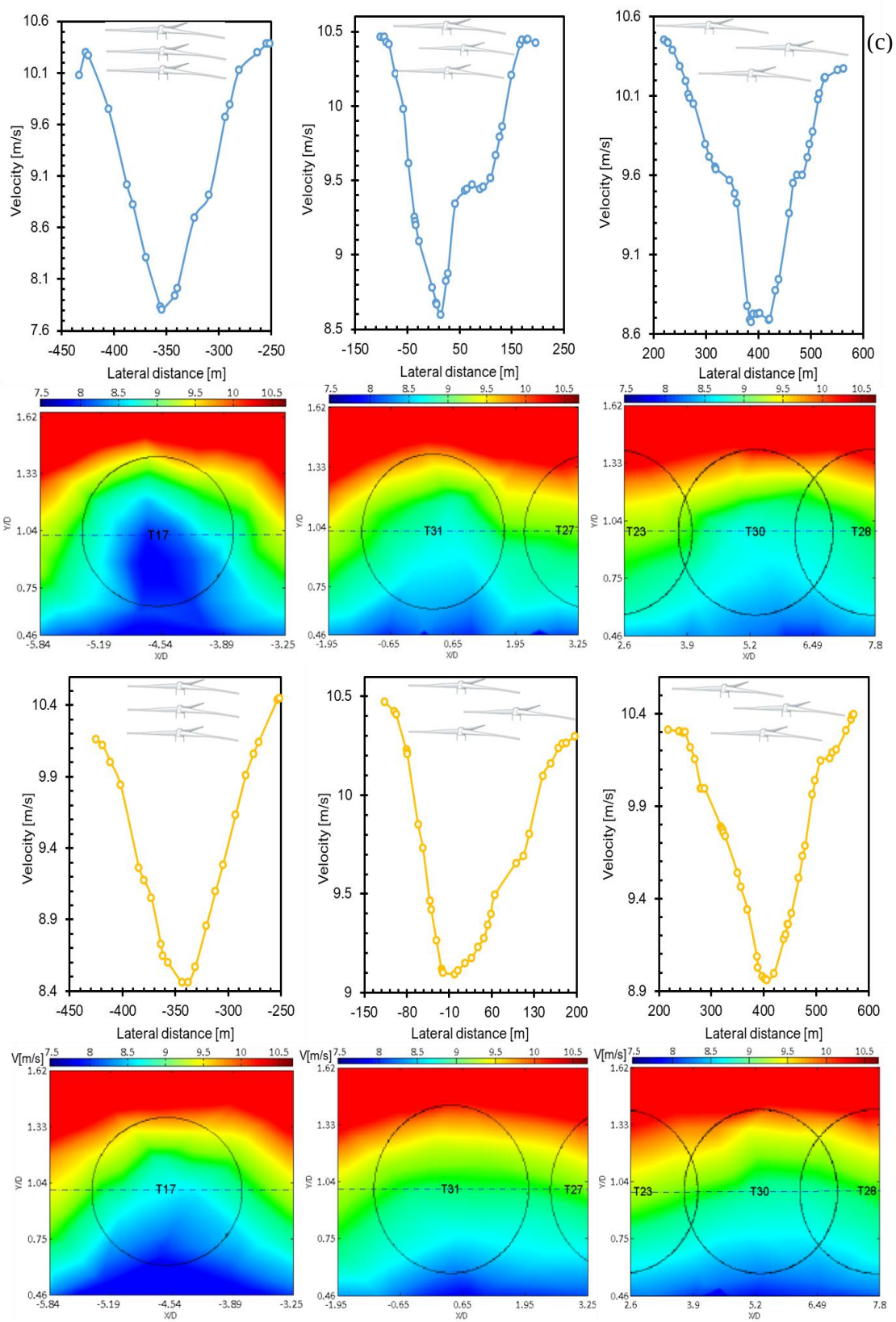

Figure 5.3: (c) velocity recovery plots and contours against lateral length of the CFD domain at downstream locations 1.5D (blue) and 6.5D (orange) of T17, T31 and T30.

5.4 The effects of compound wakes

A major objective of this research is to investigate the effects of compound wakes from the ZORLU and TGF wind farms on the FFCEL wind farm. The execution of simulations for this study included making boundary condition profiles that would exclude the incoming wake effects. The WRF based study has already simulated the region covering all three wind farms by excluding the upfront wind farms of FFCEL. Thus, the boundary condition profiles were extracted from the results of that analysis. The simulations were carried out for the cases where the turbines are placed at 60 m, 80 m, and 100 m hub heights.

Velocity contours on the plane parallel to the ground and at hub heights of the turbines and deficits in velocity and power for respective cases are given in figure 5.4. All the contours on left in Fig 5.4 present the velocity fields for all three cases where the wake effects are included in the simulations. Whereas the velocity contours on the right are the representation of flow without compound wakes. Likewise, the bar charts beneath the pair of velocity contour charts show velocity and power deficits caused by the compound wakes for each turbine. The velocity drop caused by each turbine is obvious from the abrupt change of color across the wind turbines in the velocity contours. For instance, the velocity ahead of the first-row turbines is close to 9.85 m/s at 80 m/s, which then drops to almost 8 m/s behind the disks. Another common observation across Fig 5.4 is the higher velocity deficit received by T20 and T17 for being aligned in the direction of the main wind. The lateral expansion of the wakes is yet another point of interest for wake studies. Close examination of the wakes for each turbine shows sharper cones close to the actuator disks that converge towards the principal axis of the disks. However, the lateral flow expansion from the edges of the disks shows an accelerating trend that quickly disappears. Likewise, further away in the downstream direction the wake shows moderate expansion in the lateral direction. The reason is the higher flow velocity outside of the wakes that seem to suppress the slower velocities in the wake. This is indeed a limitation of the model in that it cannot produce exact lateral expansion of the wakes. Another prominent observation validates the appropriate inclusion of location-specific velocity data to the domain. The homogenous color contours adjacent to the top and bottom lines in the charts

of velocity contours are representative of reasonable interpolation of data from a coarser grid of WRF to a finer mesh of the CFD domain.

The comparison of the velocity plots in Fig 5.4 on left with those on right for each hub height, reveals higher velocity streams for excluding wake effects. The increase of velocity across the entire domain is prominent for each case. For instance, the velocity field is dominantly color red with slight yellow patches on the right in Fig 5.4 (b). Whereas, on the left, the velocity field appears a mix of yellow and green colors. This in terms of velocity values, shows a deficit of at least 1.3 m/s for FFCEL operating in the current layout and under the effects of compound wakes. With regards to individual wakes of the turbines, we can see in both contours that the velocity behind T17 of the third row is the minimum of all the turbines. Similarly, the trend for velocity drops for each turbine is the same in both cases as the kinetic energy extracted by the disks is the same. This means that T17 in Fig 5.4 (b) left, receives a velocity magnitude of about 8.4 m/s and drops it to 7.7 m/s right aft of it. On the other hand, in Fig 5.4 (b) right, T17 has velocity inflow at the rate of 9.16 m/s and cuts it down to 8.6 m/s; the locations indicated with red dots.

The velocity and power deficit plots identify turbines in the third row of the wind farm as the most affected ones. T31 and T17 appear to produce the least powers as the effect of compound wakes are amplified by the wind turbine in upfront of them. For turbines at 60 m hub height, the velocity deficit ranges from 12.15 % to 15.17 %. This translates into power deficits in the range of 31.16 % to 38.80 %. Both velocity deficits and power deficits are predicted lesser for the existing layout of the wind farm than that of the 60 m case. Although a significant portion of the rotors operates in the direct wake of the 90 m rotors of the ZORLU wind farm, it appears that the wake recovery at higher altitudes is faster that leads to lesser impacts on downstream turbines. The velocity deficit ranges from 10.19 % to 14.06 %; interestingly the maximum velocity deficit is reported for T22 of the first row. However, the power deficit is still the highest for T31 and it is closely followed by T17 of row three. It is important to notice that the power is a function of both velocity and coefficient of power. The powers calculated here account for both, and thus higher velocity deficits might not necessarily translate into higher power deficits. The

power deficit ranges from 25.74 % to 30.95 %; where even the upper limit is less than the lower limit of power deficit in the case of 60 m. Lastly, for turbines at 100 m, the velocity deficits and power deficits are even lower than the 80m case. The velocity deficit has ranges from 8.77 % to 13.27 % and that of power deficit from 21.17 % to 28.02 %. Hence, we deduce that the effects of compound wakes are less at higher hub heights than that at lower hub heights.

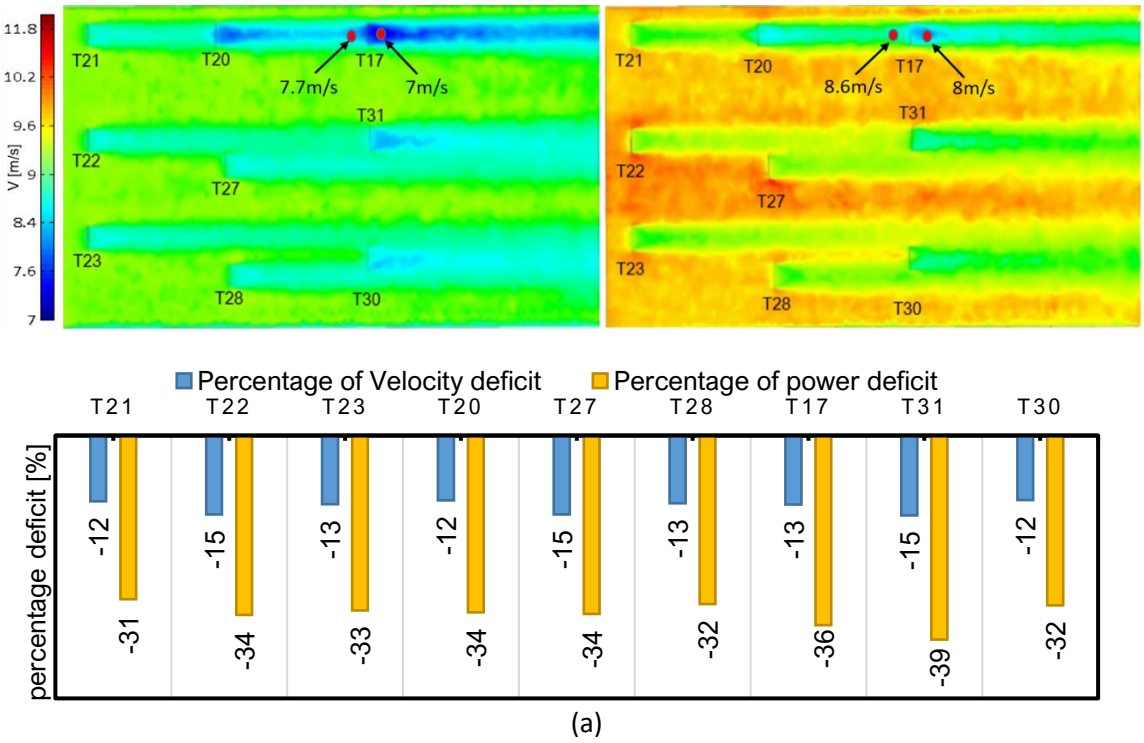

Figure 5.4: (a-left) top view of velocity field for turbines at 60 m and with the effects of compound wakes, (a-right) top view of velocity field for turbines at 60 m and without the effects of compound wakes, and (a-bottom) velocity and power deficits for each turbine.

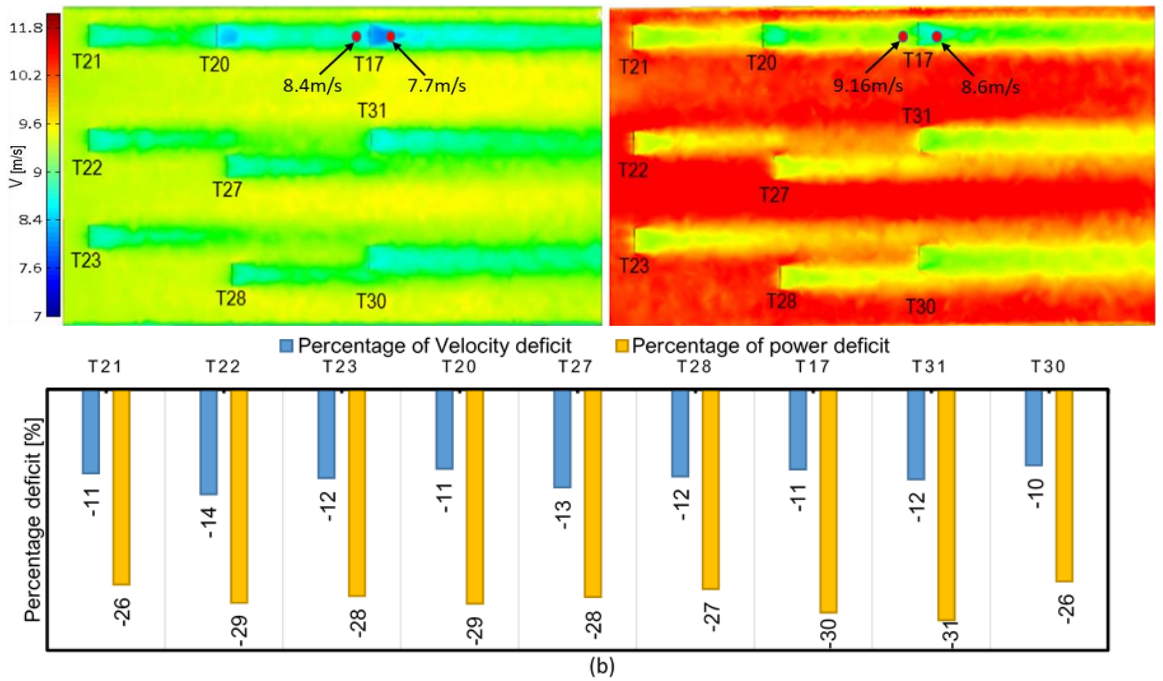

Figure 5.4: (b-left) top view of velocity field for turbines at 80 m and with the effects of compound wakes, (b-right) top view of velocity field for turbines at 80 m and without the effects of compound wakes, and (b-bottom) velocity and power deficits for each turbine.

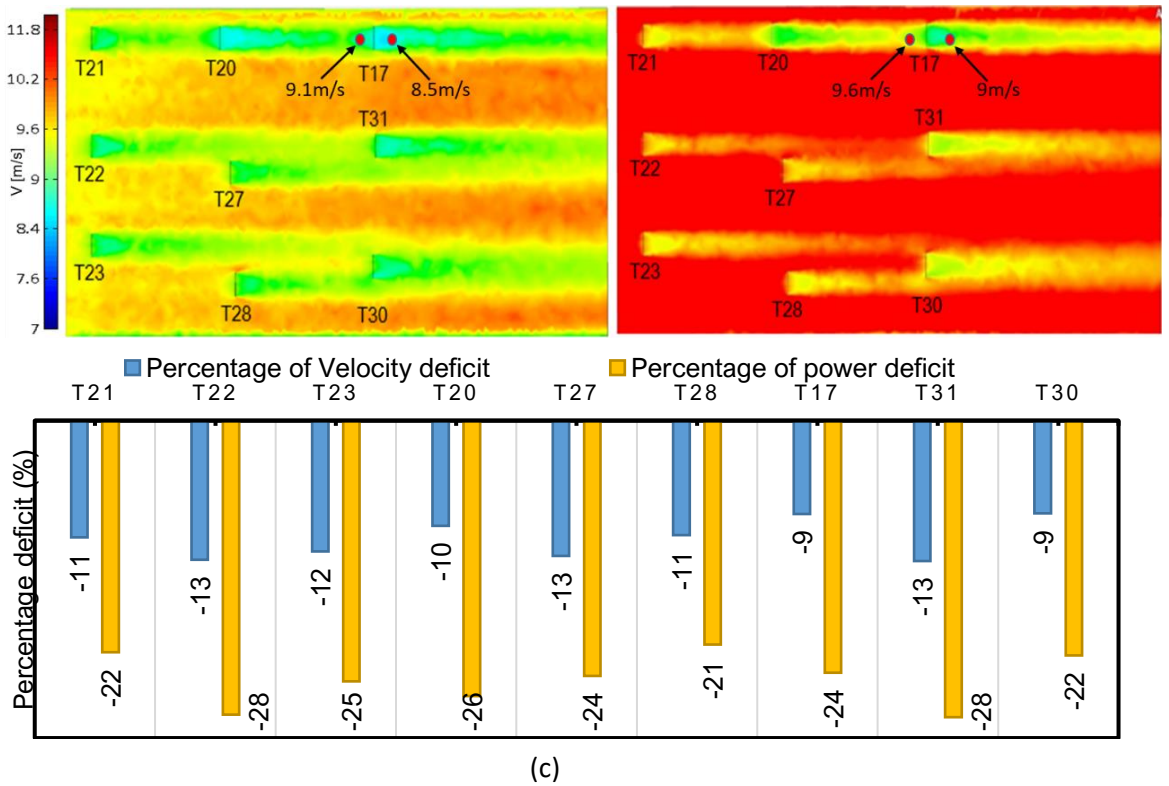

Figure 5.4: (c-left) top view of velocity field for turbines at 100 m and with the effects of compound wakes, (c-right) top view of velocity field for turbines at 100 m and without the effects of compound wakes, and (c-bottom) velocity and power deficits for each turbine.

5.5 Vertical staggering and the velocity field

The major subject of this study is to investigate the flow behavior and power variations for vertically staggering the selected 9 turbines of the FFCEL wind farm. It has been established already that the effects of compound wakes are much milder at 100m than that of both at 80 m and 60 m. Therefore, the velocity in the vertical direction is investigated in this section to further reveal the nature of flow in the sheared and convective ABL. Figure 8 presents the vertical velocity profiles for turbine T21, T20, and T17. The selection of these turbines is primarily because they are perfectly aligned in the CFD domain and reside in different rows of the three in the FFCEL wind farm. The vertical velocity profiles were plotted at two locations downstream of the same turbines. This would provide insight into the interaction of wakes with the convective and sheared ABL.

According to Fig 5.5, dropping the turbines to 60 m hub height would cause a significant drop in the velocity inflow. This is evident from the blue lines for the 60 m case lagging both orange and grey lines for 80 m and 100 m cases, respectively. Although, reducing the hub height to 60 m would release a portion of the lower rotor from the direct wakes of the larger rotors, 90 m diameter of the ZORLU wind farm. But the sheared ABL offers low velocities at such heights; this would not serve our purpose of partial repowering well. It is important to note that the velocities for the 60 m case lead both 80 m and 100 m case for heights greater than 80 m. This is because the span of rotors at 60 m would reach only 98.5 m and indeed the faster flow from such heights would accelerate into the slower flow at low heights. The same observations stand true upon comparing the vertical velocity profiles of the case 80 m with that of 100 m. However, it can be seen for the 100 m case that velocities below 100 m heights are significantly higher than that of the two other cases. Although the velocity lags for heights below 100 m but considering the average velocity across the annulus area of the rotor, the available kinetic energy still leads the other cases by a considerable margin. Also, the velocity for the 100 m cases is much closer to the rated velocity of 12.5 m/s across the span of the rotor.

The effect of staggering turbines is more beneficial for the turbines in the front row. This can be observed by the comparison of velocity values at the same heights for any of the cases under discussion. For instance, for the 100m cases, the velocity at 60 m is 9.56 m/s

at 1.5D of T21; for the same location, the velocity is 9.15 m/s for T20 and 8.94 m/s for T17 of the third row. As we switch across the rows, T21 to T20 or T20 to T17, we observe the plots more compact for the upfront turbines than that of downstream ones. Generally, the vertical velocities for lower hub heights should lag the profiles for higher hub heights. This disagreement to the general trend is identified as a limitation of the model and we can argue that the velocity deficit increases for turbines in the downstream rows and hence the implemented model's accuracy to simulate milder and turbulent streams becomes lesser. This behavior could also generate because of imposing velocities on the left and right inlets of the domain. It is unlike a conventional CFD problem that our domain has three velocity-inlet surfaces which are supplied with values across their lengths and heights.

The difference of vertical velocity field behind the same turbines at different downstream locations is evident from Fig 5.5. It can be seen from the plots for 5.5D and 6.5D locations that the higher velocities at elevated heights swipe down into the regions of lower velocities. This is the inherent structure of the ABL where the sheared velocity profile assists the recovery of the wind turbine wakes. This is justified from the decreased slops of vertical velocity curves for 5.5D and 6.5D locations, as these curves are steeper at 1.5D downstream of the turbines. Altogether, the availability of high flow velocity and better wake recovery at 100 m hub height suggests elevating the turbines to such heights for enhanced operation of the turbines affected by compound wakes.

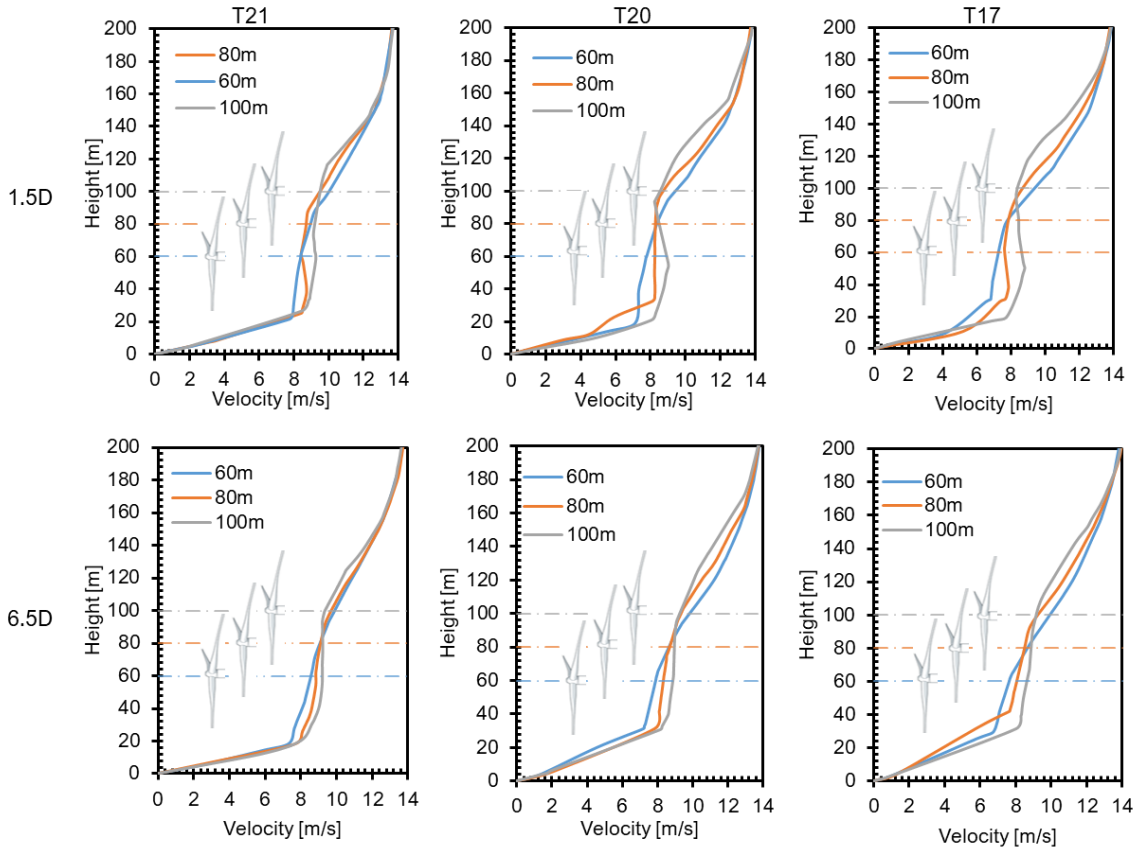

Figure 5.5: Velocity in the vertical plane at 1.5D and 6.5D locations downstream of T21, T20, and T17 at 60 m, 80 m, and 100 m.

5.6 Lateral optimization of the selecting turbines

At this stage of investigating the partial repowering of the turbines affected by compound wakes, we have found increasing hub heights as the most viable strategy for the given circumstances. It is indeed well known from the literature that the lateral spread of the wakes is much lesser than their spread in downstream directions. Thus, the wind turbines are placed closer in the lateral directions, especially when the fluctuation in the wind direction is lesser. The findings of this study have identified the turbines in partial wakes of the turbines of the same wind farm to suffer the most. Precisely, T20 and T17 are operating directly behind T21 and thus appear the most affected ones of the selected 9 turbines. Likewise, T31 is directly behind T22 and the wake of T27 has been seen to impact it partially. In the third column, T30 is affected by the wakes of T23 and T28.

Lateral positioning requires the entire turbine structures to be moved and could be the costliest strategy of the possible partial repowering methods. Nonetheless, to propose an optimized layout upon partial repowering of the wind farm, we laterally repositioned some of these 9 selected turbines. Figure 5.6 (top) shows the velocity field parallel to the ground for both actual and laterally relocated layouts. By comparing the velocity contours, we can see T20 moved out of the wake of T21. T17 was not moved as we had observed modest effects of T22 on to T31, which are also aligned but kept significantly away in the downstream direction. The improved velocity inflows to T17 and T20 are much enhanced, which is obvious on the chart on the right of Fig 5.6 (top). To set T31 free of the wake of T27, we slightly moved it down in the lateral direction only. Again, the separate wake cones of T27 and T31 are prominent on the velocity contour chart on the right. It was noticed earlier that T30 is affected by T28 more than that by T23. Thus, we moved T23 upwards in the domain and dragged T28 downwards to release T30 of the wake effects. Once again, the distinct wake of T28 can be seen away from T30 but that of T23's tail still falls onto it. The effects of the wake of T23 should be minimum for the considerable downstream distance between T30 and T23. It is important to note that this lateral positioning was constrained by the availability of space because there are more turbines on both sides of these 9 turbines in the lateral direction.

The power comparison for the actual and laterally optimized layout is given in Fig 5.6 (bottom). The bars represent the powers for both the laterally relocated case and the actual case, where all the turbines are at 100m hub heights. The front row of the turbines is not relocated and thus the powers perfectly match for both cases. For the rest of the turbines, the powers have increased significantly, with T28 showing the most promising hike. The incoming velocity for each turbine is in between 9 m/s and10 m/s, for which the turbines are rated to produce powers in the range of 1000 kW to 1200 kW. It is obvious from the powers estimated for the laterally relocated turbines that they produce powers close to their rated values and higher than the actual layout.

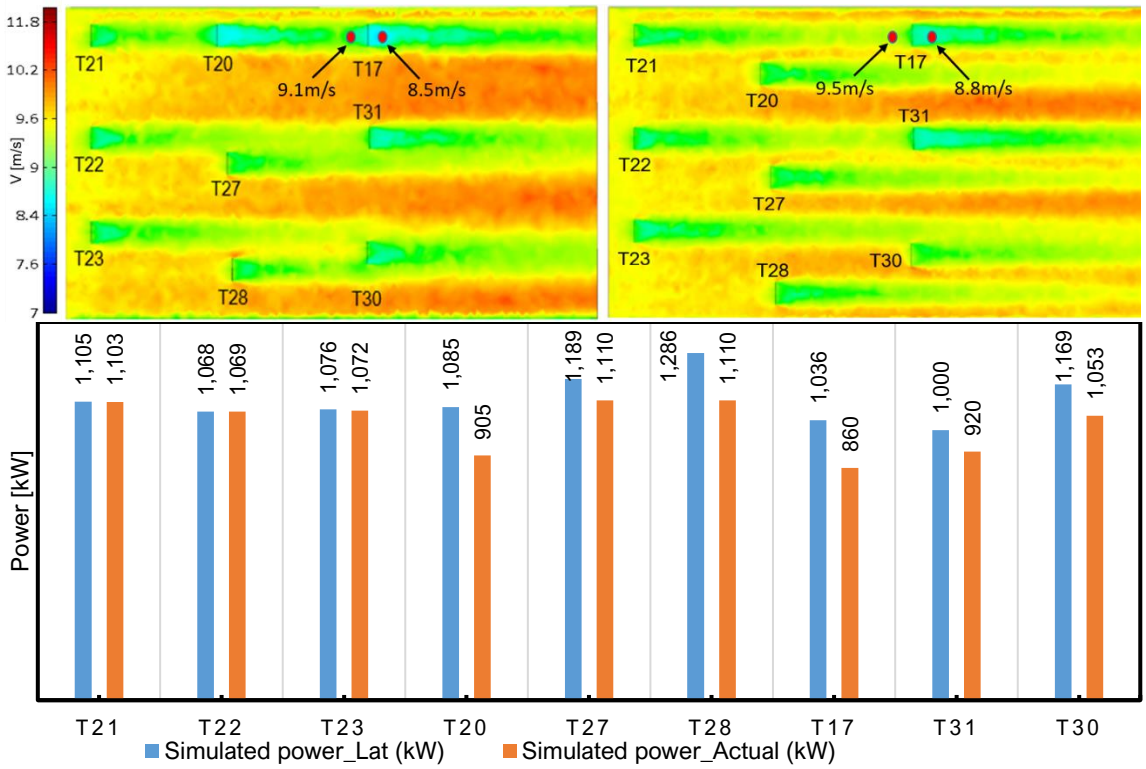

Figure 5.6: (top-left) velocity contours for the turbines at 100 m hub height and in current lateral locations, (top-right) velocity contours for laterally repositioned layout, and (bottom) comparison of powers for the laterally relocated case and actual case.

Summary

This chapter presented the analyses of the simulations performed for the CFD study of the FFCEL wind farm. The first analysis validated the model by comparing the power characteristics of the selected turbines predicted by the CFD model with that of the WRF predictions. The impact of the stability of the atmosphere on the recovery of the wake is the second subject of interest. Where the convective atmospheric conditions prove beneficial to wake recovery. In the third analysis, we considered the wake propagation and interaction of each of the selected turbines. This identified T20 and T17 as the most affected turbines among the selected 9. A major objective of the thesis is to inspect the impacts of the compound wakes on the FFCEL wind farm. This was discussed in the fourth section of this chapter. The effects of compound wakes were observed more at lower hub heights and thus turbines at higher hub heights receive fewer impacts. We then proceeded to vertical staggering in the fifth part, where the pros and cons of changing hub heights are analyzed. This analysis suggested increasing the hub heights to 100 m from 80m. Finally, the lateral reposition of the selected turbines for an optimized layout was discussed in the last analysis of this chapter. A case of the 9 turbines at 100 m was simulated by relocating some of them laterally. The optimized layout now included both vertical and lateral repositioning of the turbines and thus suggested up to a 23 % increase in power output over that of the current configuration.

Chapter 6

Conclusions and Recommendations

6.1 Conclusions

This study considered vertical staggering as a strategy to partially repower the FFCEL wind farm in Jhimpir, Pakistan. The compound wakes from ZORLU and TFC wind farms affect the performance of the FFCEL farm and therefore an affordable mid-life repowering strategy of the wind farm was investigated. A mesoscale numerical study for the same wind farm identified the most affected turbines and we picked 9 of those turbines for a micro-scale numerical study. We investigated the effects of compound wakes on vertically staggered layouts by decreasing the hub heights to 60m and then increasing it to 100m. Further, a convective atmospheric boundary layer was also included to imitate a close to the real wind farm environment.

For the RANs, boundary condition data were interpolated from the results of the WRF study for the site. Some modifications to the coefficients of the k-e turbulence model, the wall roughness model, and the buoyancy model were made based on recommendations in the literature to mimic the convective ABL for a real wind farm. Following are some of the major conclusions of the research.

(1) The comparison of the simulated powers for the 9 turbines at all three hub heights reveals 100 m being the most desirable hub height. The cumulative power output of turbines at 60 m hub height is 7.194 MW, which is 6.306 MW less than the rated 1.5x9 = 13.5 WM. Likewise, the turbines in the current state, 80 m hub height appear to produce 8.13MW power that is 5.37 MW less than the rated power but 0.936 MW more than the 60 m case. For turbines at 100 m hub height, the sum of simulated power is 9.21 MW. This lags the rated power by only 4.29 MW but exceeds by 1.08 MW and 2.016 MW to that of at 80 m and 60 m cases, respectively.

(2) The effects of compound wake of the upfront wind farms appear to affect the turbines at low heights more than those at elevated heights. A case study was carried out by moving the turbines to both 60 m and 100 m from 80 m and observe the influence of the compound wakes for each configuration.

(3) Each case was simulated for both with the incoming wakes and without the wakes. We noticed that the turbines at 60 m were affected the most, followed by those at 80 m. The 100 m case showed the least impacts of compound wakes.

(4) Further, the recovery of the compound wakes through the wind farm was fastest for turbines placed at 100m.

(5) We also compared the wake recovery profiles of the same turbines for neutral ABL and convective ABL to figure out that wakes recover faster in the convective ABL.

(6) Increasing the hub heights of the turbines and then laterally relocating the turbines in direct wakes of the upstream turbines leads to impressive hikes in the power output. The power output increased by 23 % of the current configuration for turbines at 100 m and some of them relocated.

6.2 Way forward

Although this research presents the promising potential to adopt vertical staggering as a method for partially repowering the wind farms affected by the intra-farm wakes, more improvements are needed to enhance the proposed strategy. The inclusion of small vertical axis wind turbines below the lower heights of the rotor blade tips could also prove vital to harvesting the flow stream close to the ground. The use of more accurate wind turbine resolving schemes like ALM and ASM should be considered for future work. The inclusion of more parameters governing the stability of the atmospheric boundary layer is also required. Moreover, the use of LES platforms is strongly recommended to understand the propagation of the compound wakes and their interaction with the turbines at small length scales. An economic analysis for the vertically staggered wind farms should also be considered to evaluate their financial feasibility.

Acknowledgment

Firstly, I would like to thank Allah Almighty for providing me knowledge, determination, opportunity, and strength to complete this venture. Without His blessings, all of it would not have been possible.

I would like to express my gratitude to my supervisor Dr. Sehar Shakir for allowing me to conduct my thesis under her supervision.

I would also like to thank my co-supervisor Dr. Adeel Javed for providing guidance and motivation throughout the research and study.

I also want to thank my GEC committee members Dr. Majid Ali and Dr. Warda Ajaz. I feel proud and honored that you have accepted to be on my committee.

I wish to acknowledge Syed Haseeb and FFCEL for providing the required data for the project.

Finally, and most importantly, I express my profound gratitude to my parents for providing me with unfailing support and continuous encouragement throughout my years of study and through the process of researching and writing this thesis.

Appendix A: The profile files for boundary conditions

A sample of profiles formatted to assign the boundary conditions is given below. The data was taken from the WRF simulations done for the site. By careful positioning of the coordinates of the wind turbines and boundaries of the CFD the data were interpolated to the CFD mesh.

((vel_profrw	mesh	1	160	0)			
(x							
-445	-455	-445	-445	-445	-445	-445	-445
-445	-445	-445	-445	-445	-445	-445	-445
-445	-445	-455	-445	-445	-445	-445	-445
-445	-455	-445	-445	-445	-445	-445	-445
-445	-455	-445	-445	-445	-445	-445	-445
-445	-445	-445	-445	-445	-445	-445	-445
-445	-445	-455	-445	-445	-445	-445	-445
-445	-455	-445	-445	-445	-445	-445	-445
-445	-455	-445	-445	-445	-445	-445	-445
-445	-445	-445	-445	-445	-445	-445	-445
-445	-445	-455	-445	-445	-445	-445	-445
-445	-455	-445	-445	-445	-445	-445	-445
-445	-455	-445	-445	-445	-445	-445	-445
-445	-445	-445	-445	-445	-445	-445	-445
-445	-445	-455	-445	-445	-445	-445	-445
-445	-455	-445	-445	-445	-445	-445	-445
-445	-455	-445	-445	-445	-445	-445	-445
-445	-445	-445	-445	-445	-445	-445	-445
-445	-445	-455	-445	-445	-445	-445	-445
-445	-455	-445	-445	-445	-445	-445	-445)
(y							
0.00E+00	0.00E+00	0.00E+00	0.00E+00	0.00E+00	0.00E+00	0.00E+00	0.00E+00
1.00E+01	1.00E+01	1.00E+01	1.00E+01	1.00E+01	1.00E+01	1.00E+01	1.00E+01
2.00E+01	2.00E+01	2.00E+01	2.00E+01	2.00E+01	2.00E+01	2.00E+01	2.00E+01
3.00E+01	3.00E+01	3.00E+01	3.00E+01	3.00E+01	3.00E+01	3.00E+01	3.00E+01
4.00E+01	4.00E+01	4.00E+01	4.00E+01	4.00E+01	4.00E+01	4.00E+01	4.00E+01
5.00E+01	5.00E+01	5.00E+01	5.00E+01	5.00E+01	5.00E+01	5.00E+01	5.00E+01
6.00E+01	6.00E+01	6.00E+01	6.00E+01	6.00E+01	6.00E+01	6.00E+01	6.00E+01
7.00E+01	7.00E+01	7.00E+01	7.00E+01	7.00E+01	7.00E+01	7.00E+01	7.00E+01
8.00E+01	8.00E+01	8.00E+01	8.00E+01	8.00E+01	8.00E+01	8.00E+01	8.00E+01
9.00E+01	9.00E+01	9.00E+01	9.00E+01	9.00E+01	9.00E+01	9.00E+01	9.00E+01
1.00E+02	1.00E+02	1.00E+02	1.00E+02	1.00E+02	1.00E+02	1.00E+02	1.00E+02
1.10E+02	1.10E+02	1.10E+02	1.10E+02	1.10E+02	1.10E+02	1.10E+02	1.10E+02
1.20E+02	1.20E+02	1.20E+02	1.20E+02	1.20E+02	1.20E+02	1.20E+02	1.20E+02
1.40E+02	1.40E+02	1.40E+02	1.40E+02	1.40E+02	1.40E+02	1.40E+02	1.40E+02
1.60E+02	1.60E+02	1.60E+02	1.60E+02	1.60E+02	1.60E+02	1.60E+02	1.60E+02
1.80E+02	1.80E+02	1.80E+02	1.80E+02	1.80E+02	1.80E+02	1.80E+02	1.80E+02
2.00E+02	2.00E+02	2.00E+02	2.00E+02	2.00E+02	2.00E+02	2.00E+02	2.00E+02
2.20E+02	2.20E+02	2.20E+02	2.20E+02	2.20E+02	2.20E+02	2.20E+02	2.20E+02
2.40E+02	2.40E+02	2.40E+02	2.40E+02	2.40E+02	2.40E+02	2.40E+02	2.40E+02
2.50E+02	2.50E+02	2.50E+02	2.50E+02	2.50E+02	2.50E+02	2.50E+02	2.50E+02)
(z							

-1.00E+02	-3.00E+02	-5.00E+02	-7.00E+02	-9.00E+02	-1.10E+03	-1.30E+03	-1.50E+03
-1.00E+02	-3.00E+02	-5.00E+02	-7.00E+02	-9.00E+02	-1.10E+03	-1.30E+03	-1.50E+03
-1.00E+02	-3.00E+02	-5.00E+02	-7.00E+02	-9.00E+02	-1.10E+03	-1.30E+03	-1.50E+03
-1.00E+02	-3.00E+02	-5.00E+02	-7.00E+02	-9.00E+02	-1.10E+03	-1.30E+03	-1.50E+03
-1.00E+02	-3.00E+02	-5.00E+02	-7.00E+02	-9.00E+02	-1.10E+03	-1.30E+03	-1.50E+03
-1.00E+02	-3.00E+02	-5.00E+02	-7.00E+02	-9.00E+02	-1.10E+03	-1.30E+03	-1.50E+03
-1.00E+02	-3.00E+02	-5.00E+02	-7.00E+02	-9.00E+02	-1.10E+03	-1.30E+03	-1.50E+03
-1.00E+02	-3.00E+02	-5.00E+02	-7.00E+02	-9.00E+02	-1.10E+03	-1.30E+03	-1.50E+03
-1.00E+02	-3.00E+02	-5.00E+02	-7.00E+02	-9.00E+02	-1.10E+03	-1.30E+03	-1.50E+03
-1.00E+02	-3.00E+02	-5.00E+02	-7.00E+02	-9.00E+02	-1.10E+03	-1.30E+03	-1.50E+03
-1.00E+02	-3.00E+02	-5.00E+02	-7.00E+02	-9.00E+02	-1.10E+03	-1.30E+03	-1.50E+03
-1.00E+02	-3.00E+02	-5.00E+02	-7.00E+02	-9.00E+02	-1.10E+03	-1.30E+03	-1.50E+03
-1.00E+02	-3.00E+02	-5.00E+02	-7.00E+02	-9.00E+02	-1.10E+03	-1.30E+03	-1.50E+03
-1.00E+02	-3.00E+02	-5.00E+02	-7.00E+02	-9.00E+02	-1.10E+03	-1.30E+03	-1.50E+03
-1.00E+02	-3.00E+02	-5.00E+02	-7.00E+02	-9.00E+02	-1.10E+03	-1.30E+03	-1.50E+03
-1.00E+02	-3.00E+02	-5.00E+02	-7.00E+02	-9.00E+02	-1.10E+03	-1.30E+03	-1.50E+03
-1.00E+02	-3.00E+02	-5.00E+02	-7.00E+02	-9.00E+02	-1.10E+03	-1.30E+03	-1.50E+03
-1.00E+02	-3.00E+02	-5.00E+02	-7.00E+02	-9.00E+02	-1.10E+03	-1.30E+03	-1.50E+03
-1.00E+02	-3.00E+02	-5.00E+02	-7.00E+02	-9.00E+02	-1.10E+03	-1.30E+03	-1.50E+03
-1.00E+02	-3.00E+02	-5.00E+02	-7.00E+02	-9.00E+02	-1.10E+03	-1.30E+03	-1.50E+03)
(k							
0.00E+00	0.00E+00	0.00E+00	0.00E+00	0.00E+00	0.00E+00	0.00E+00	0.00E+00
1.34E-01	1.33E-01	1.33E-01	1.32E-01	1.34E-01	1.33E-01	1.32E-01	1.31E-01
1.46E-01	1.42E-01	1.42E-01	1.39E-01	1.40E-01	1.39E-01	1.36E-01	1.35E-01
1.53E-01	1.48E-01	1.48E-01	1.44E-01	1.43E-01	1.43E-01	1.39E-01	1.39E-01
1.55E-01	1.50E-01	1.50E-01	1.46E-01	1.44E-01	1.44E-01	1.40E-01	1.41E-01
1.56E-01	1.51E-01	1.51E-01	1.47E-01	1.44E-01	1.45E-01	1.42E-01	1.42E-01
1.58E-01	1.52E-01	1.52E-01	1.49E-01	1.45E-01	1.47E-01	1.43E-01	1.44E-01
1.60E-01	1.53E-01	1.53E-01	1.51E-01	1.45E-01	1.48E-01	1.44E-01	1.45E-01
1.62E-01	1.54E-01	1.54E-01	1.53E-01	1.45E-01	1.48E-01	1.45E-01	1.46E-01
1.65E-01	1.55E-01	1.55E-01	1.55E-01	1.46E-01	1.49E-01	1.47E-01	1.47E-01
1.68E-01	1.57E-01	1.57E-01	1.57E-01	1.48E-01	1.50E-01	1.48E-01	1.49E-01
1.72E-01	1.61E-01	1.61E-01	1.62E-01	1.53E-01	1.54E-01	1.53E-01	1.54E-01
1.78E-01	1.70E-01	1.70E-01	1.72E-01	1.67E-01	1.68E-01	1.68E-01	1.68E-01
1.84E-01	1.80E-01	1.80E-01	1.82E-01	1.80E-01	1.80E-01	1.81E-01	1.79E-01
1.89E-01	1.84E-01	1.84E-01	1.87E-01	1.85E-01	1.84E-01	1.85E-01	1.84E-01
1.93E-01	1.89E-01	1.89E-01	1.91E-01	1.90E-01	1.88E-01	1.89E-01	1.88E-01
1.98E-01	1.94E-01	1.94E-01	1.96E-01	1.94E-01	1.93E-01	1.94E-01	1.93E-01
2.02E-01	1.99E-01	1.99E-01	2.00E-01	1.98E-01	1.97E-01	1.98E-01	1.97E-01
2.05E-01	2.02E-01	2.02E-01	2.04E-01	2.02E-01	2.01E-01	2.02E-01	2.01E-01
2.06E-01	2.04E-01	2.04E-01	2.05E-01	2.04E-01	2.03E-01	2.04E-01	0.2030123
(V							
0.00E+00	0.00E+00	0.00E+00	0.00E+00	0.00E+00	0.00E+00	0.00E+00	0.00E+00
7.63E+00	7.61E+00	7.61E+00	7.52E+00	7.63E+00	7.58E+00	7.60E+00	7.63E+00
9.04E+00	8.85E+00	8.85E+00	8.75E+00	8.77E+00	8.65E+00	8.72E+00	8.72E+00
9.89E+00	9.61E+00	9.61E+00	9.50E+00	9.44E+00	9.30E+00	9.43E+00	9.43E+00
1.01E+01	9.83E+00	9.83E+00	9.71E+00	9.54E+00	9.46E+00	9.66E+00	9.71E+00
1.03E+01	9.99E+00	9.99E+00	9.86E+00	9.55E+00	9.56E+00	9.83E+00	9.91E+00
1.05E+01	1.01E+01	1.01E+01	9.99E+00	9.55E+00	9.64E+00	9.98E+00	1.01E+01
1.07E+01	1.03E+01	1.03E+01	1.01E+01	9.60E+00	9.72E+00	1.01E+01	1.02E+01
1.09E+01	1.04E+01	1.04E+01	1.03E+01	9.69E+00	9.82E+00	1.03E+01	1.04E+01
1.12E+01	1.06E+01	1.06E+01	1.05E+01	9.84E+00	9.96E+00	1.04E+01	1.06E+01
1.15E+01	1.09E+01	1.09E+01	1.07E+01	1.01E+01	1.02E+01	1.07E+01	1.08E+01

1.18E+01	1.13E+01	1.13E+01	1.11E+01	1.07E+01	1.07E+01	1.11E+01	1.13E+01
1.23E+01	1.19E+01	1.19E+01	1.18E+01	1.16E+01	1.16E+01	1.18E+01	1.19E+01
1.27E+01	1.26E+01	1.26E+01	1.25E+01	1.25E+01	1.25E+01	1.25E+01	1.26E+01
1.30E+01	1.29E+01	1.29E+01	1.29E+01	1.29E+01	1.28E+01	1.29E+01	1.29E+01
1.33E+01	1.32E+01	1.32E+01	1.31E+01	1.31E+01	1.31E+01	1.32E+01	1.32E+01
1.35E+01	1.34E+01	1.34E+01	1.34E+01	1.34E+01	1.34E+01	1.34E+01	1.34E+01
1.38E+01	1.37E+01	1.37E+01	1.37E+01	1.37E+01	1.37E+01	1.37E+01	1.37E+01
1.40E+01	1.39E+01	1.39E+01	1.39E+01	1.39E+01	1.39E+01	1.39E+01	1.39E+01
1.41E+01	1.40E+01	1.40E+01	1.40E+01	1.40E+01	1.40E+01	1.40E+01	14.002223)

Appendix B: Journal Paper

Partial Repowering Analysis of a Wind Farm by Coupled Actuator Disk and Mesoscale Models to Mitigate Neighboring Wind Farm Wake Interference

Mehtab Ahmad Khan[a], Adeel Javed[a,2], Sehar Shakir[a], Abdul Haseeb Syed[b]

[a]U.S.-Pakistan Centre for Advanced Studies in Energy (USPCAS-E), National University of Sciences and Technology (NUST), H-12 Islamabad, Pakistan

[b]Department of Wind Energy, Technical University of Denmark (DTU), Rosklide, Denmark

Abstract

This study explores the partial repowering of a commercial-scale wind farm with deteriorated performance under the influence of wakes originating from upstream wind farms. The case study considers a total of 9 out of 33 most deteriorated wind turbine generators (WTGs) for a microscale computational fluid dynamics (CFD) analysis using the steady-state actuator disk model (ADM) coupled with the boundary condition data from the mesoscale weather research and forecasting (WRF) model. Furthermore, the convective atmospheric boundary layer (ABL) has also been considered for the investigation. The baseline predicted power at 80m hub height has been validated by the observed data for each of the 9 x WTGs. Both vertical and horizontal staggering options have been assessed for partial repowering and recovery of the generation output. Initially, the hub heights have been varied to 60m and 100m and compared to the baseline at 80m in separate cases. By elevating the turbines to 100 m hub height, the cumulative power generation from the 9 x WTGs increased by approximately 13.5% while reducing the hub height to 60m decreases the power output by approximately 11.5% of that of the current configuration at 80m hub height. The effect of the compound wakes appeared mild at 100m, modest at 80m, and high at 60m; as the maximum velocity deficit observed under the influence of compound wakes is approximately 13.3%, 14.1%, and 15.2%, respectively. Further lateral repositioning is applied to the 3 x WTGs identified as the most wake affected even after the vertical staggering to 100m hub height resulting in a final cumulative power increase of up to 23% compared to the existing layout. This paper hence presents an applied insight for partial repowering of onshore wind farms affected by intra- and inter-farm compound wakes.

Keywords: commercial wind farm; partial repowering; actuator disk model; compound wake interferences; model validation; vertical and horizontal staggering.

[2]Corresponding author, Adeel Javed, Ph.D., Email: adeeljaved@uspcase.nust.edu.pk